Novel resorbable glass-ceramic scaffolds for hard tissue engineering: from the parent phosphate glass to its bone-like macroporous derivatives

Novel resorbable glass-ceramic scaffolds for hard tissue engineering: from the parent phosphate glass to its bone-like macroporous derivatives

Oana Bretcanu[1], Francesco Baino[2], Enrica Verné[2] and Chiara Vitale-Brovarone[2,*]

[1] *School of Mechanical and Systems Engineering, Newcastle University, Stephenson Building, Claremont Road, Newcastle upon Tyne, NE1 7RU, United Kingdom.*

[2] *Institute of Materials Physics and Engineering, Applied Science and Technology Department, Politecnico di Torino, Corso Duca degli Abruzzi 24, 10129 Torino, Italy.*

* Corresponding author: Chiara Vitale-Brovarone

Tel: +39 011 090 4716

Fax: +39 011 090 4624

E-mail: chiara.vitale@polito.it

Abstract

One of the major challenges of hard tissue engineering research focuses on the development of scaffolds that can match the mechanical properties of the host bone and resorb at the same rate as the bone is repaired. The aim of this work was the synthesis and characterization of a resorbable phosphate glass, as well as its application for the fabrication of 3-D scaffolds for bone regeneration. The glass microstructure and behaviour upon heating were analyzed by X-ray diffraction, differential scanning calorimetry and hot stage microscopy. The glass solubility was investigated according to relevant ISO standards using distilled water, simulated body fluid (SBF) and Tris-HCl as testing media. The glass underwent progressive dissolution over time in all three media but the formation of a hydroxyapatite-like layer was also observed on the samples soaked in SBF and Tris-HCl, which demonstrated the bioactivity of the material. The glass powder was used to fabricate 3-D macroporous bone-like glass-ceramic scaffolds by adopting polyethylene particles as pore formers: during thermal treatment, the polymer additive was removed and the sintering of glass particles was allowed. The obtained scaffolds exhibited high porosity (87 vol.%) and compressive strength around 1.5 MPa. After soaking for 4 months in SBF, the scaffolds mass loss was 76 wt.% and the pH of the solution did not exceed the 7.55 value, thereby remaining in a physiological range. The produced scaffolds, being resorbable, bioactive, architecturally similar to trabecular bone and exhibiting interesting mechanical properties, can be proposed as promising candidates for bone repair applications.

Keywords

Scaffold; Phosphate glass; Resorbable material; Macroporous glass-ceramic; Bone tissue engineering.

Introduction

Restoration and healing of bone defects by using bioactive materials is one of the major topics of research in hard tissue regenerative medicine. Silicate bioactive glasses have been the subject of intense interest for the last three decades due to their ability to form *in vitro* and *in vivo*, when exposed to physiological fluids, a surface apatite layer having the capacity to strongly bond to the surrounding host tissue [1-6]. A selected number of such glasses, e.g. 45S5 Bioglass® and 13-93 glass, have received the approval for clinical use in Europe and USA and have shown great success in many dental and orthopaedic applications [7]. However, there are still some issues related to the long-term effect of released silica [8] and the quite slow degradation kinetics of these biomaterials, often taking many years to disappear from the body before being completely replaced by natural tissue [9,10]. Because of these limitations, the search for new materials for the repair of bone defects has continued over the years and has led to the development of phosphate-based glasses as valuable alternatives [11]. Phosphate glasses, basically belonging to the P_2O_5–CaO–Na_2O system, have unique dissolution properties in aqueous fluids [12]. Degradation rates can be varied from hours to several weeks by properly designing the glass composition and, furthermore, these glasses can be synthesised to include metal ions that are able to induce a specific biological effect ranging from enhanced osteoblast activity to antibacterial properties [13-15]. In common with silicate-based glasses, the building block of phosphate glasses is a tetrahedral unit (PO_4); however, the PO_4 unit is quite different from the SiO_4 unit [16]. In fact, phosphate glasses are formed by PO_4 tetrahedra that can be attached to a maximum of three neighbouring units forming a 3-D network; the oxygen atoms that are not shared between phosphate tetrahedra allocate their two unpaired electrons with the P^{5+} ions to form a terminal double bond. The fact that phosphate anions contain at least one terminal oxygen limits the connectivity of phosphate-based glasses

in comparison to their silicate-based counterparts. Pure vitreous silica (SiO_2) is thermally and chemically stable; the addition of modifying oxides, such as Na_2O, K_2O, MgO and CaO, which are not part of the glass network and disrupt it, resulting in terminal Si–O bonds, produces less stable glasses. On the contrary, pure vitreous phosphorus pentoxide (P_2O_5) is chemically unstable with regard to hydrolysis of the P–O–P bonding by atmospheric moisture; in this case, the addition of metal oxides improves its stability because $P–O–M^+$ bonds (where M = alkali or alkali earths cation) are generally more stable towards atmospheric hydrolysis. With respect to silicate glasses, phosphate-based systems can be prepared at relatively low melting temperatures and can easily be drawn into fibres; thanks to this feature, use of phosphate glasses in soft tissue engineering for production of conduits for peripheral nerve regeneration [17,18] or muscle tissue regeneration [19] has been proposed. Compared to silicate glasses, phosphate glasses have poor chemical durability and low mechanical properties; however, their application in the context of bone tissue engineering offers interesting perspectives thanks to their compositional versatility. By purposely tailoring the glass composition, it is possible to develop glasses having dissolution rate compatible with the kinetics of new bone formation; furthermore, phosphate glasses can act as carriers for the controlled release of oligo-elements exerting specific therapeutic actions *in vivo* [20].

In the context of tissue engineering, biomedical glasses have been also used for the fabrication of 3-D porous scaffolds. An ideal scaffold for bone grafting should fulfil a complex set of requirements, including high porosity (above 50 vol.%, i.e. comparable to that of cancellous bone), macropores size exceeding 100 μm, highly interconnected 3-D porous network, mechanical strength matching that of host bone, bioresorbability rate similar to that of bone regeneration and biocompatibility of the degradation products [1,3,21-24]. Different methods have been proposed to produce bioceramic scaffolds, including starch consolidation [25,26], H_2O_2 foaming [27], gel-casting [28,29], sponge replication [30-35], sponge replication

combined with gel-casting [36] and polymer particles burning-out [37-40]. The above-mentioned methods were widely applied over the last decade to process fully-crystalline ceramics, such as hydroxyapatite (HA) or β-tricalcium phosphate (β-TCP), or silicate glasses; however, to the best of the authors' knowledge few attempts to process phosphate glasses in porous form have been reported in the literature. In 2004, Navarro et al. [41] described the preparation of P_2O_5-CaO-Na_2O-TiO_2 scaffolds by H_2O_2 foaming; two years later, Park et al. [42] illustrated the synthesis of CaO-CaF_2-P_2O_5-MgO-ZnO scaffolds by using the sponge replication technique. More recently, in a couple of articles Vitale-Brovarone et al. [43,44] proposed the fabrication of P_2O_5-SiO_2-CaO-MgO-Na_2O-K_2O scaffolds by the foam replica method; phosphate glass/gelatin composite scaffolds with bilayered structure have been also proposed for ostechondral regeneration [45].

In the present work, phosphate glass-ceramic scaffolds were fabricated by the burning-out method using polyethylene (PE) particles as pore forming agent, in order to obtain porous bodies with mechanical strength comparable to that of cancellous bone. PE burning-out method is applied here for the first time to fabricate phosphate glass-derived scaffolds. An accurate investigation of the starting glass was also reported, especially as far as its sintering and crystallization upon heating and its solubility in physiological media are concerned; these analyses were not systematically performed previously and the knowledge of such characteristics is essential for a rational development of glass-derived scaffolds. Microstructural and morphological characterizations of the scaffolds were carried out by X-ray diffraction and scanning electron microscopy, respectively; scaffolds porosity, solubility in different media and mechanical properties were also determined.

Materials and methods

Starting glass

Glass synthesis. The starting glass, referred to as ICEL2, is a 6-oxide glass having the following molar composition: 45% P_2O_5, 3% SiO_2, 26% CaO, 7% MgO, 15% Na_2O and 4% K_2O. ICEL2 was prepared by using the following high-purity raw products: $Na_3PO_4 \cdot 12H_2O$, $Ca_3(PO_4)_2$, SiO_2, $(NH_4)_2HPO_4$, $Mg_3(PO_4)_2 \cdot 8H_2O$ and K_2HPO_4 (Sigma-Aldrich). The reagents were ground in a ball mill for 1 h to ensure good mixing and then melted in a platinum crucible at 1200 °C for 30 minutes in air (heating rate: 10 °C min^{-1}). The melt was poured into rectangular shape brass moulds at room temperature to obtain glass bars. A part of the ICEL2 glass bars was annealed at 375 °C for 12 h, whereas the residual bars was ground in powders. Annealing reduced the internal stresses induced by rapid cooling, thereby avoiding the formation of cracks during slicing the glass bars. The annealed bars were cut into small slices (around 10 mm × 10 mm × 1.2 mm) by using a cutting machine (Struers Secotom-10) with a diamond cut-off wheel. The glass slices were further used for the solubility tests. The non-annealed bars were ground for 1 h in a ball mill and the obtained powder was then sieved below 106 μm by using stainless steel sieves (Giuliani Corp., Italy). The so-obtained ICEL2 glass powder was finally used to prepare the porous scaffolds, as described in the section 2.2).

Microstructural and thermal analysis. X-ray diffraction (XRD) pattern of ICEL2 glass powder was registered by a Philips X`Pert diffractometer with Cu K_α radiation for a 2θ range within 10-70° (Bragg-Brentano camera geometry; working conditions: 40 kV and 30 mA; incident wavelength: 0.15405 nm).

The characteristic temperature of ICEL2, i.e. glass transition temperature (T_g), onset crystallization temperature (T_x), peak crystallization temperature (T_c) and melting temperature

(T_m), were determined by a Perkin Elmer DSC7 differential scanning calorimeter, in argon atmosphere, using a heating rate of 10 ° C min^{-1}.

The sintering process of ICEL2 was directly observed by hot stage microscopy (HSM), that allows the quantification of the sintering parameters by measuring the variation of the samples dimensions during the heating process. The behaviour of the samples during heating was analyzed by a Leitz-Wetzlar heating stage optical microscope in air atmosphere, using a heating rate of 10 °C min^{-1}. The samples were obtained by pressing ICEL2 powder into small cubes (3-mm edge length) using a small stainless steel die. The specimens were observed by a video-camera and the photos of their silhouettes were registered up to 700 °C. The samples shrinkage was calculated at specific temperatures from the variation of the samples area, using the following equation:

$$\text{shrinkage}(\%) = \frac{A_T}{A_0} \times 100 \quad (1)$$

wherein A_0 (mm^2) was the initial area of the specimen silhouette at room temperature and A_T (mm^2) was the area of the specimen silhouette at the temperature T.

Solubility tests. The glass solubility was tested at 37 °C on glass slices by using three different solutions, i.e. distilled water, simulated body fluid (SBF) and Tris-HCl as recommended by ISO standard [46], for a total soaking time of 4 months. SBF was prepared by using Kokubo's protocol [47]. Tris-HCl is a solution obtained by dissolving tris-hydroxymethylamino methane ($NH_2C(CH_2OH)_3$) in distilled water, followed by regulating the pH at 7.4 by using 1 M HCl. ICEL2 slices were immersed in 15 ml of each solution at 37 °C in PE bottles. The solutions were refreshed twice a week and the pH was measured before refreshing. The samples were removed from each solution after different soaking time and let to dry in air. The weight of the samples was measured before and after soaking; the weight loss was calculated with the following equation:

$$\text{weight loss}\,(\%) = \frac{W_0 - W_t}{W_0} \times 100 \qquad (2)$$

wherein W_0 (g) is the initial weight of the specimen and W_t (g) is the weight of the specimen at the immersion time t.

The tests were performed on triplicate samples, and the presented weight losses are an average of the acquired data. The weight loss per unit surface was calculating by dividing the weight loss by the initial surface area of the specimens. Some selected samples were chromium-coated and investigated by scanning electron microscopy (SEM; Philips 525M, accelerating voltage 15 kV) and energy dispersive spectroscopy (EDS; Philips Edax 9100) for compositional analysis.

Glass-derived scaffolds

Scaffolds fabrication. ICEL2-based scaffolds were fabricated using the PE burning-out method. This method involved the preparation of green bodies by mixing PE particles (Wrigley Fibres Co. Ltd, UK) and ICEL2 glass powders, as reported elsewhere by the authors for silicate glass scaffolds [37-39]. Briefly, a homogeneous blend of PE particles (50 vol.%; particle size between 100-300 μm) and ICEL2 glass powder (particles size below 106 μm) was obtained by using a tube roller (mixing time: 1 h). The mixture was then pressed into a cylindrical stainless steel mould (diameter: 30 mm) by using a uniaxial press (applied stress: 120 MPa). The obtained green body discs were thermally treated at 550 °C for 3 h in air atmosphere (heating rate: 10 °C min^{-1}) in order to have the complete removal of the organic phase and the sintering of the inorganic particles. The sintering temperature was properly selected on the basis of the HSM data.

Microstructural and morphological characterization. ICEL2-derived scaffolds were crushed in fine powders and analyzed by XRD (according the operating conditions reported in the section 2.1.2) to investigate the development of crystalline phases; X'Pert HighScore program and PCPDFWIN database (JCPDS - International Centre for Diffraction Data) were used for identification.

The scaffolds 3-D architecture was analysed by SEM according to the experimental set-up described in the section 2.1.3.

Porosity assessment. The total porosity of the scaffolds was calculated with the following equation:

$$\mathrm{P}\,(\%) = \left(1 - \frac{\rho_s}{\rho_g}\right) \times 100 \tag{3}$$

wherein ρ_s (g cm^{-3}) is the scaffold density (measured from mass-volume evaluations) and ρ_g (g cm^{-3}) is the ICEL2 bulk glass density (measured by exploiting the Archimedes's principle, using a density kit attached to an analytical balance). The porosity was expressed as mean value ± standard deviation calculated on 10 samples.

Quantitative assessment of pores size distribution was carried out by image analysis (Qwin Leica software) on low-magnification SEM pictures of polished cross-sections of the scaffolds (three images were considered for each measurement). This program enhances the difference in contrast between the "empty space" (pores) and "filled space" (struts) and calculates the number of pores within a specific size range, as well as their surface area. The pores, identified by black colour, were approximated as spherical by the software; hence, the equivalent pore radius R (μm) is calculated from the formula:

$$\mathrm{R} = \sqrt{A_p / \pi} \tag{4}$$

where A_p (μm^2) is the pore area measured by the program.

The degree of interconnectivity was estimated from a qualitative viewpoint by observing the absorption of a red coloured fluid by the scaffolds due to capillary forces. For this purpose, a mix composed by 30 vol.% of calf serum and distilled water was prepared as a testing medium; few drops of red ink were added to the serum solution for better visualization. The bottom part of the scaffold was put in contact with this red serum solution and the time required for the penetration of the liquid inside the scaffold and up to its top was registered.

Mechanical tests. The strength of the scaffolds was evaluated through crushing tests on 10 mm × 10 mm × 10 mm cubic samples (MTS System Corp. apparatus, 5-kN cell load, cross-head speed set at 1 mm min^{-1}). The compressive failure stress σ_c (MPa) was calculated as

$$\sigma_c = \frac{L_M}{A_R}, \tag{5}$$

being L_M (N) the maximum load registered during the test and A_R (mm^2) the resistant section area.

The energy per unit volume E_V (J mm^{-3}) absorbed by the scaffold till the breaking off is reached was defined as the energy necessary to deform a specimen from the unloaded condition to the failure strain ε_f, and was calculated as the area under the stress-strain curve up to ε_f [48]:

$$E_V = \int_0^{\varepsilon_f} \sigma(\varepsilon) d\varepsilon, \tag{6}$$

wherein the strain ε is the integration variable; the initial condition is $\sigma(\varepsilon = 0) = 0$ and the final state is $\sigma(\varepsilon = \varepsilon_f) = \sigma_c$ (calculated from Eq.(5)).

The above-mentioned mechanical parameters were expressed as mean value ± standard deviation calculated on five samples.

In vitro tests. The scaffolds solubility was assessed only in SBF, being this solution recognized by the scientific community as the "gold standard" medium for assessment of biomaterials behaviour *in vitro*. ICEL2-based scaffolds were soaked in 15 ml of SBF at 37 °C in PE bottles for a time span of 4 months. The solution was refreshed twice a week and the pH was registered before refreshing. The weight was measured before and after different soaking time and the weight loss was calculated with Eq.(2). The tests were performed on triplicate samples, and the presented weight losses are an average of the acquired data. At the end of the experiment, some samples were gently washed with distilled water, dried at room temperature, chromium-coated and investigated by SEM and EDS (experimental set-up described in the section 2.1.3.).

Results and discussion

Parent phosphate glass

Considerations on the design of glass composition. ICEL2 was developed by modifying the chemical composition of an experimental silicate glass named CEL2 and proposed by the authors for biomedical applications since the mid 2000s [31,33,37,49,50]. The oxide-based formulations of ICEL2 and CEL2 can be considered "specular" [43], as the molar amounts of SiO_2 and P_2O_5 in the ICEL2 composition were inverted in comparison to those of CEL2; the so-obtained phosphate glass is characterized by small silica content and no variation of the amounts of modifying oxides, as well as of the former/modifying oxides molar ratio, with respect to CEL2 composition.

The integration of modifying oxides into the phosphate glass composition has a significant effect on the glass structure and its dissolution rate, contributing to improve its resistance to

hydrolysis [11,16]. Ca and Mg ions also play an important role from a biological standpoint, as they are involved in bone metabolism and are known to stimulate osteoblasts proliferation and new bone growth [51].

Concerning the effect of SiO_2, i.e. the co-former oxide of ICEL2 together with P_2O_5, it was demonstrated that it breaks the phosphate glass network, which results in an increased degradation rate [52]. Incorporation of silica in ICEL2 formulation is essential considering the specific applications of the glass in regenerative medicine: in fact, it has been reported that SiO_2 increases the Ca nodule formation in osteoblasts cultures and seems to stimulate the osteoblasts differentiation [29,53]. More generally, it has been demonstrated that the dissolution products of bioactive glasses exert a genetic control over the osteoblasts cycle, and silicon was found to play a key role in bone mineralization and gene activation towards a path of osteogenesis and self-repair [51,53].

Sintering and crystallization of the glass. The XRD pattern of as-poured ICEL2 is shown in Fig. 1a; the presence of a broad halo indicates a completely amorphous phase. The amorphous halo, which is characteristic of glass samples, can be observed for 2θ between 20-40°.

DSC curve of ICEL2 glass powder is reported in Fig. 2. The glass transition temperature occurs at T_g = 410 °C. The graphic presents a large exothermic peak whose maximum is around T_c = 600 °C and two small endothermic peaks between 650-700 °C. The exothermic peak corresponds to crystallization phenomena (the crystallization onset was detected at T_x = 550 °C), while the two endothermic peaks represent a double melting process (i.e., melting of two crystalline phases). The broadness of the exothermic peak suggests the crystallization of two phases, as observed from XRD pattern in Fig. 1b (described in more detail in the section 3.2.1) and in accordance with the detection of two melting temperatures by DSC.

Glass stability against crystallization upon heating can be evaluated, from a quantitative viewpoint, by considering the following difference estimated from DSC plot (Fig. 2):

$$\delta = T_x - T_g \tag{7}$$

This parameter indicates the tendency towards crystallization of the glass composition, as a greater difference reveals a lower tendency to crystallization, i.e. a greater stability of the material in its vitreous state upon heating. In the case of ICEL2 we had δ = 140 °C.

Hruby [54] proposed another parameter, K_H, defined as

$$K_H = \frac{T_x - T_g}{T_m - T_x} \tag{8}$$

that can be used to measure glass stability. According to Hruby, the larger K_H of a certain glass, the greater its stability against crystallization upon heating. In the case of ICEL2 we assessed K_H = 1.4.

ICEL2 glass shrinkage as a function of increasing temperature is shown in Fig. 3. The sample exhibited no geometrical variation up to T_{FS} = 350 °C (first shrinkage) and then it began to contract; the shrinkage reached its maximum (60 %) at T_{MS} = 470 °C (maximum shrinkage). For temperatures higher than T_{EP} = 550 °C (end of the densification plateau) the sample volume increased due to crystallization phenomena, in good agreement with DSC results. The maximum increase of the volume was reached at 620 °C; afterwards the material, that was converted into a glass-ceramic, started to melt.

Lara et al. [55] recently introduced a new parameter, S_c (sinterability), that estimates the competition between glass sintering and crystallization of glass powders during heating:

$$S_c = T_x - T_{MS} \tag{9}$$

It represents a measure of the ability of sintering versus crystallization: the greater S_c, the more independent are the kinetics of these two processes. Specifically, S_c can be interpreted according to these general criteria: if $S_c < 0$, only partial densification is achieved before

crystallization begins; otherwise, if $S_c \geq 0$, full densification occurs prior to crystallization. Therefore, higher S_c are related to higher final densities, which indicated a better sintering behaviour involving a higher densification of the final sample. In the case of ICEL2, we obtained $S_c = 80$ °C.

Table 1 gives a comparison among the thermal parameters calculated for ICEL2 in the present work and those available in the literature for other biomedical glasses. To the best of the authors' knowledge, unfortunately, no comparison among ICEL2 and other phosphate-based glasses is directly possible (CEL2 [34], 45S5 Bioglass® [56] and the glasses investigated by Kansal et al. [57] are all silicate materials). The parameters related to glass stability against crystallization and sinterability of ICEL2 are superior than those of its specular counterpart CEL2, as well as of 45S5 Bioglass®.

Before discussing about ICEL2-derived scaffolds, few considerations about the selection of the optimal sintering temperature deserve to be reported here. As a general guideline, data from thermal analyses are helpful to biomaterials researchers for choosing the most appropriate sintering temperature to produce glass-derived scaffolds; this selection is commonly carried out with the aim of obtaining a good compromise between densification, required to strengthen the struts of the final porous body, and porosity, which is recommended to be above 50 vol.% in order to promote cell colonization, implant vascularisation and bone in-growth *in vivo* [24,29]. However, it is worth underlining that the sintering process of scaffolds obtained by PE burning-out, like those fabricated in this work, is quite different from the sintering of compact bodies of glass powder, like those used for HSM. In fact, during thermal treatment of the glass/PE green bodies we assist not only to densification/crystallization of glass particles, but also to the burning-out of the polymeric additive, which may introduce additional shrinkage or expansion (due to gas development) of the structure. Furthermore, PE particles leave large macro-voids in the 3-D scaffold structure

to be consolidated during sintering, whereas the pores detectable in compact bodies of glass powders are attributable to small intra-particulate voids. From a theoretical viewpoint, HSM of a glass/PE compact body would maybe give more accurate information to select the optimal sintering temperature for scaffolding, but for purpose of simplicity such an approach has been never followed neither in the literature nor in the present work. In the authors' opinion this choice is fully acceptable, also considering that, although HSM can certainly provide a range of potentially suitable sintering temperatures, the "optimal" sintering temperature can be found only through a fine evaluation involving the production, thermal treatment and morphological investigation of some test samples; this issue was already discussed elsewhere by the authors with reference to sponge-replicated scaffolds [34].

As a general criterion, the sintering temperature should be chosen in the range between the maximum densification and the onset of crystallization; therefore, the sintering temperatures to be selected for ICEL2 are in the 470-550 °C range, wherein the best densification can be obtained. The optimal thermal treatment for ICEL2 scaffold fabrication was selected at T_{EP} = T_x = 550 °C for 3 h in air atmosphere. For temperatures lower than 550 °C, the organic phase was not completely burnt-out and the scaffold structure was only partial sintered (the sintering took place in solid state), which ensued in high brittleness and weak mechanical properties. Increasing the temperature, the glass viscosity decreased and at 550 °C viscous flow sintering occurred, which allowed the glass particles to be bound together into a structure with a higher density. Adopting thermal treatments above 550 °C, the scaffold structure partially collapsed due to a high degree of melting.

In vitro tests. Digital camera images of ICEL2 glass slices before and after soaking for 4 months in three different media (distilled water, Tris-HCl and SBF) are shown in Fig. 4. As can be noticed, the samples immersed in Tris-HCl (Fig. 4b) and SBF (Fig. 4c) had a white

layer on top of them after immersion. This layer was identified by EDS analysis as a calcium phosphate (CaP), which precipitated during the soaking period. In fact, as previously reported by other authors [58], when the dissolution time raises, the release of phosphates in the solution increases and, in media such as SBF, the saturation occurs rapidly thereby leading to the precipitation of a HA-like phase. Due to the presence of a newly formed CaP layer, the weight losses that occurred in these two solutions (Tris-HCl and SBF) were underestimated. On the contrary, as can be observed in Fig. 4a, no precipitation of new phases occurred on the sample soaked in distilled water, and thus its area and thickness were much smaller than those of the samples maintained in Tris-HCl and SBF. The precipitation of this CaP layer, similar to the apatite phase present in the natural bone [59,60], indicates a bioactive behaviour of ICEL2 glass.

Fig. 5 reports the weight loss in the three different media up to 4 months of soaking. As can be noticed, the glass dissolution increased over time in all media and had a significantly higher rate for distilled water. For instance, the weight loss after 4 months of immersion in distilled water reached almost 76 wt.%, while the samples soaked in Tris-HCl and SBF lost only 21 wt.% and 29 wt.%, respectively, of their initial own weight. This variation among the groups can be explained by considering the precipitation of the CaP layer on the samples surface during the immersion in SBF and Tris-HCl, as its presence partially balanced the weight loss due to stoichiometric dissolution of polyphosphate chains. Furthermore, the presence of this CaP layer slowed down the hydrolysis of the phosphate glass as its direct contact with water molecules is partially hindered by the precipitated layer acting as a "protecting skin". However, the dissolution rate was higher than the CaP precipitation rate, and therefore a weight loss was registered also for the samples soaked in Tris-HCl and in SBF.

The average weight loss per unit surface of ICEL2 glass samples after different time of immersion in distilled water is presented in Fig. 6 (continuous line). The coefficient of determination $R^2 = 0.9981$ of the linear fitting curve $y = 1.7114x$ (dashed line) indicates a very good fitting (correlation coefficient R = 0.99905). The linear trend suggests a homogeneous (congruent) dissolution of the glass due to surface erosion; this is consistent with current knowledge on phosphate glasses that are considered erosion-controlled systems, in accordance with a kinetic limited by the dissolution of the hydrated polyphosphate chains [61]. According to the fitting curve equation, the ICEL2 dissolution rate in water was constant and equal to about 1.7 mg cm^{-2} day^{-1}. The dissolution remained linear with time as the test solution was periodically replenished; in this condition, the ionic strength of the solution was kept nearly constant, otherwise an increase of the ionic strength would have caused a decrease of the dissolution rate [61].

An approximately linear trend of weight loss with time was also observed for the Tris-HCl group; in this medium, the dissolution rate was less than the one observed in distilled water, due to the precipitation of the CaP layer, as previously discussed. In the case of SBF, the situation was more complex: the dissolution rate was nearly linear over the first 14 days of immersion, then decreased tending to zero and after 1 month increased again with a linear trend (also in this case the dissolution rate was lower than that registered in distilled water). It is possible to hypothesize that, after this time span, the CaP layer (or even only some regions of it) reached a critical thickness, thereby tending to detach from the substrate glass; accordingly, the removal of this "physical barrier" would involve an acceleration of the dissolution rate. The chelating ability of increasing concentration of polyphosphate ions in solution towards divalent cations in the hydrated layer of the glass might also have enhanced the dissolution process, as suggested by Gao et al. [59].

Phosphate glass-derived scaffolds

Microstructure, architecture and morphology. A digital image of a pressed glass/PE disc (green body) before sintering is shown in Fig. 7a. During the thermal treatment the glass crystallized and, therefore, the obtained scaffolds had a glass-ceramic microstructure (Fig. 1b). Two crystalline phases, i.e. $Na_2Mg(PO_4)_3$ and $Ca_2P_2O_7$, were identified from XRD analysis, in good agreement with the DSC curve (Fig. 2) showing two melting peaks that corresponded to the above-mentioned crystalline phases. Phase identification is also consistent with the results reported elsewhere by the authors [62]. It should be taken into account that the sintered ICEL2 constituting the macroporous scaffolds is actually a glass-ceramic material; however, for purpose of simplicity the expression "ICEL2 scaffold" will be adopted hereafter, without further specifying its glass-ceramic nature.

During the heat treatment, the ICEL2 glass particles sintered and the PE particles burnt-out producing a grey smoke. The removal of the gaseous products occurred in the same time with the glass softening and thus the green body discs remarkably swelled during the thermal treatment. The obtained scaffolds had the height up to 3 times larger than that of the starting green bodies and looked like a "cake" (Fig. 7b). The grey colour of the sintered scaffolds was due to the presence of some carbon residuals (not completely eliminated owing to the relatively low sintering temperature) entrapped in the structure during the passage of the smoke through the sample; compositional analysis by EDS revealed that carbon traces are negligible. The gases produced during PE pyrolysis flowed up from the bottom to the top of the samples, thereby contributing to create a macroporous structure with a 3-D interconnected network of pores that can be easily observed by naked eye (Fig. 7c). The scaffolds microstructure is shown in Fig. 7d. The SEM image reveals the presence of both macropores (size in the 100-400 μm range) and micropores (< 20 μm) exhibiting a good degree of

interconnectivity. In general, the pores wall structure is very well sintered. At 550 °C, the surface of the glass particles was in a viscous state; this viscous fluid produced at the interface between the glass particles created a better contact between the adjacent glass particles, thereby driving to the formation of a highly sintered structure (Fig. 7d).

The scaffold porosity calculated by mass-volume measurements was 87 ± 3 vol.%. Percentage porosity is a key parameter to preliminarily estimate the suitability of a given scaffold for tissue engineering application; for instance, a total porosity above 50 vol.% is generally recommended for bone tissue scaffolds [24]. However, other parameters such as pores size, distribution and interconnectivity deserve careful consideration in the process of scaffold design and development.

The capillarity test performed on a ICEL2 scaffold to qualitatively investigate the interconnectivity of its pores is shown in Fig. 8. The scaffolds could absorb the red serum in a couple of seconds; the fast uptake was due to the presence of a network of highly interconnected micropores and to their capillarity effect on the fluid (Figs. 8a-f). Scaffolds before and after the capillarity test are displayed in Figs. 8g,h: qualitative observations of the scaffold surface and cross-section showed a uniform red colour, which further confirmed the existence of a porous network with a high degree of interconnectivity.

The features of the pore network will influence permeability, which will affect how body fluids penetrate into the scaffold as well as the rate of cell migration and vascularised bone in-growth. In the present work, the intrinsic permeability k (m^2) in Darcy's flow region was estimated by using the following equation [63]:

$$k = \frac{D^2 \xi^3}{150 \cdot (1-\xi)^2} \tag{10}$$

wherein D (m) is the mean pore diameter and ξ is the effective porosity.

The effective porosity ξ, whose values are in the 0-1 range, is defined as the fractional volume of pore space that permits the fluid flow; it is different from the absolute porosity P (assessed by Eq.(3)), which is defined as the percentage of total void space with respect to the bulk volume regardless of the interconnection of the pore voids. The mean pore diameter D refers to the effective porosity ξ and was estimated by image analysis (Qwin Leica software) excluding from the calculation the pores with size below 10 μm, as they constituted only a sort of surface roughness on the scaffold struts; several cross-sectional low-magnification SEM images of ICEL2 scaffolds were analyzed for this purpose. Likewise, the parameter ξ was estimated subtracting the contribution of the small pores below 10 μm from the total pores content P. The estimates of D and ξ were ~40 μm and ~0.84, respectively. It cannot be ignored that such evaluations represent only an approximate assessment of the real values of the parameters since image analysis provides results that refer to a 2-D geometry (cross-sectional pictures of the samples were processed), whereas a more realistic analysis of scaffold porosity should be carried out in 3-D. However, this simplified approach is generally considered acceptable by researchers and has been followed in the literature for preliminary investigation of porous glass biomaterials [33,34,44] as it is able to lead to quite reliable results [64]. Therefore, by using Eq.(10) the estimate of ICEL2 scaffolds permeability was $k = 2.47 \cdot 10^{-10}$ m^2. It is interesting to compare the value of permeability assessed for the present ICEL2 scaffolds with data available in the literature. In the case of bone, for instance, values between $k = 2.0 \cdot 10^{-9}$ and $k = 9.5 \cdot 10^{-9}$ m^2 have been reported for cancellous bovine bone with ξ in the 80-90 vol.% range [65]. Values of $k = 7.22 \cdot 10^{-9}$ and $k = 5.13 \cdot 10^{-9}$ m^2 have been found for human trabecular bone of the vertebral body and proximal femur, respectively, although significant variation from these values may be obtained dependent of the harvest site and local porosity [66]. Shimko et al. [67] found values of intrinsic permeability in the range $k = 5.2 \cdot 10^{-10}$-$6.2 \cdot 10^{-10}$ m^2 for tantalum scaffold having porosity within 90-95 vol.%. Li et al. [68]

established $k = 2.13 \cdot 10^{-10}$ m^2 for calcium phosphate scaffolds, and more recently Ochoa et al. [69] reported $k = 1.96 \cdot 10^{-9}$ m^2 for 45S5 Bioglass® foams with porosity above 90 vol.%. The estimate of permeability for ICEL2 scaffolds is comparable to the range of the reported experimental data for trabecular bone and bone tissue engineering scaffolds, confirming that the produced samples are interesting structures for bone repair.

At present, studies reporting the evaluation of biomedical scaffolds permeability are quite rare in the literature, probably due to the complexity of the approaches to be followed for its evaluation. Experimental measurements of permeability in biomaterials with 3-D interconnected porous networks can be very difficult if the considered materials are highly brittle, like the majority of biomedical glass and ceramic scaffolds; furthermore, the development of a purposely-dedicated measurement system is needed [63,69]. An alternative method for measuring the permeability of sol-gel glass scaffolds was proposed by Jones et al. [70,71] and involved the use of 3-D geometry of the porous sample obtained via micro-computed tomography (micro-CT) in a microscale flow simulation. The flow within porous medium obeys Stokes equations at the local scale; hence, the permeability can be calculated using the geometry and by numerically solving a Stokes-like problem obtained by volume averaging. This technique has a great potential as it allows non-destructive observations of areas of dominant flow within an individual scaffold; however, the need for a micro-CT equipment implies high cost for the analysis and the development of a purposely-dedicated software may be necessary; furthermore, the analysis can be dramatically time-consuming.

More accurate measurements of ICEL2 scaffolds permeability are planned in the future to refine the present estimate.

Mechanical properties. A typical compressive stress-strain curve of ICEL2 scaffold is shown in Fig. 9. The failure compressive strength was 1.5 ± 0.5 MPa; in the light of the suggestions

from the literature, this value can be considered acceptable for applications in the context of bone tissue engineering, being close to the lower threshold of the strength range of trabecular bone (2-12 MPa [72]). The achievement of such a compressive strength is a significant result in the light of the high porosity of these scaffolds (about 87 vol.%): their porosity/resistance ratio is actually comparable to that of some natural materials (e.g. cancellous bone, but also coniferous tree wood) or artificial structures for advanced applications (e.g. aluminium honeycomb).

As far as the authors are aware, the mechanical strength of the ICEL2 scaffolds produced in this work is superior to that of biomedical glass scaffolds with analogous porosity reported in the literature. For instance, it is interesting to notice that 45S5 Bioglass® scaffolds, having a pore content of 85-90 vol.% and often considered as a standard reference to which compare new macroporous bioglasses, exhibit a compressive strength around 0.3-0.4 MPa [30], which is significantly lower than that of the ICEL2 scaffolds presented in this work. A compressive strength of 1.5 MPa was achieved for highly porous (85 vol.%) 45S5 Bioglass® foams after toughening by means of a polymeric coating [73].

The present ICEL2 scaffolds produced by PE burning-out are also stronger than those made of the same material but fabricated by the authors elsewhere through sponge replication method (~0.4 MPa [43,44]). This trend can be observed for all existing biomedical glass scaffolds that were produced by these two different methods, as shown in Table 2. From a general viewpoint, in the scaffolds produced by PE burning-out the pores are separated by thick struts without the presence of an actual bone-like trabecular structure with very thin struts characterizing the samples manufactured through replication method: therefore, the higher mechanical strength is negatively counterbalanced by an architecture somewhat different than the one featuring cancellous bone and by a lower degree of pore interconnectivity.

The ICEL2 scaffolds investigated in this work, although being produced by PE burning-out, nevertheless exhibit a bone-like morphology with a high degree of pores interconnectivity; such characteristics were reasonably due to the simultaneous glass particles softening/sintering and PE removal during the thermal treatment, which induced the "foaming" of the structure (Fig. 7b). This phenomenon does not occur for silicate glass scaffolds (Table 2) as they need a higher temperature of sintering (normally above 900 °C): therefore, first PE particles burn-out and then glass particles sintering occurs (the two processes are "decoupled"), which eventually ensues in a shrinkage of the scaffold.

By decreasing the pores content (porosity of 50 vol.% minimum is recommended for bone scaffolds [24]), which can be performed by introducing a lower amount of PE particles in the starting glass/PE mix, it would be possible to further increment the mechanical strength of the ICEL2 scaffolds, whose use could be maybe suggested also for load-bearing applications.

In spite of the high pore content, the scaffolds can be easily cut with a blade without crumbling (Fig. 7c); this supports their use for clinical applications, as surgeons would be able to safely handle and to carve them into the desired shape without breaking.

The energy absorption capacity was calculated from the area under the stress-strain curve; specifically, the energy absorbed by the scaffold up to its breaking off was $E_V \sim 150$ kJ m^{-3}. This value is about one order of magnitude higher than that assessed for ICEL2 scaffolds produced by sponge replication [44] and might be further increased up to 20 times by the incorporation of biopolymers, as demonstrated by recent literature on bioceramic/polymer porous composites [74-76]. Furthermore, the scaffold toughness will increase *in vivo*: for instance, porous HA scaffolds, with a brittle response as fabricated, showed an elastoplastic response in compression after implantation for 8 weeks in pigs [77]. In general, upon implantation of a bioactive/resorbable glass scaffold in a bone defect, the strength of the scaffold decreases with time due to conversion of the glass to an HA-like material and/or its

progressive degradation, but this should be countered by an increase in strength due to bone in-growth [78].

In vitro behaviour. The weight losses of ICEL2 scaffolds after different time frames of immersion in SBF are presented in Fig. 10. After soaking for 4 months the samples lost almost 76 wt.%. This value is about 2.5 times higher than the one obtained for glass slices; although the glass slices were totally amorphous and thus more prone to dissolution than ICEL2 in its glass-ceramic form, the scaffold had a higher surface area exposed to SBF and, accordingly, its reactivity was emphasized. During the treatment in SBF the scaffold volume underwent a progressive reduction but the sample did not collapse; this characteristic is quite important as some porous biomaterials dramatically crumble during dissolution, thereby losing their structural function. This observation is consistent with the mechanism of congruent erosion during contact with aqueous solutions that characterizes phosphate glass-based biomaterials.

Figs. 11a,b show the SEM micrographs of the scaffolds before and after immersion in SBF for 2 months. After soaking the pores became larger and the wall struts between the pores became thinner. Some of the pores walls opened during dissolution, thereby leading to pores widening and creation of additional interconnects among them; this suggests that the possible presence of closed pores in ICEL2 scaffolds before implantation *in vivo* will not represent a dramatic aspect *per se*, as they will open during scaffold dissolution. Fig. 11c reports a high-magnification SEM image of scaffold struts after soaking for 2 months in SBF. The presence of a newly formed phase, partially closing the small pores on the surface of scaffold struts, can be observed. These CaP agglomerates partially coated the scaffold surface, thereby making almost undetectable the peaks corresponding to the elements peculiar of scaffold composition (Na, Mg, K, Si) in the EDS pattern (Fig. 11d). Therefore, ICEL2 scaffolds were

not only resorbable but also bioactive according to the relevant mechanism described by Hench [72].

Quantitative assessment of pores distribution before and after the treatment in SBF confirmed what suggested by SEM micrographs (Fig. 11): in fact, image analysis evaluations performed on several low-magnification SEM images demonstrated that after soaking in SBF the total pores amount and total pores area increased of about 31 and 36 %, respectively. Pores number and pores area distributions are displayed in Fig. 12, wherein the results are normalized and expressed in percentage to make easier the comparison of the values before and after immersion in SBF. This analysis clearly shows that, due to congruent dissolution of the scaffolds, the amount of both small (< 50 μm) and large pores (> 100 μm) increased; therefore, the mean pore diameter (about 15 μm) referred to overall porosity P remained unaltered before and after the treatment in SBF. Likewise, also the ratios among the pores amount and pores area for each class of pore size exhibited moderate differences between the two conditions.

Adhesion and proliferation of osteoblasts as well as the formation of mineralized tissue depends on the extracellular pH regulation [79]. The pH variation of the SBF during the 4-month time span of soaking of ICEL2 scaffolds was within the range for the normal function of bone cells (maximum reached value: pH = 7.55) [79].

An extensive biological characterization of ICEL2 was carried out elsewhere by the authors [44,62] and, accordingly, is not reported in the present work. Very briefly, human marrow stromal cells seeded on this biomaterial maintained their metabolic activity and ability to proliferate (over a 21-day test period); furthermore, cells differentiation over proliferation occurred, thereby suggesting potential osteogenic properties of the scaffolds.

By looking at the future, investigations in dynamic conditions and/or by using bioreactors (*in vivo*-like environment) would provide key information in view of the final *in vivo* application

of the material. In fact, for degradable scaffolds, like those based on phosphate glasses including ICEL2, the rate of flow through the material will affect the degradation rate. More specifically, differences in flow rate within a scaffold can cause differential degradation rates, and for resorbable glass scaffolds areas with higher flow rates are likely to degrade more rapidly than areas of low flow. Fluid will always flow along the route of least resistance; flow will occur around the edge of the sample as well as through it, and preference flow channels may form as material dissolves under the flow rates required for measurement [71]. During *in vitro* cell culture, the flow of culture medium containing cells during cell seeding is critical to developing an evenly populated scaffold. *In vivo*, it is vital that there are paths for cells to migrate, tissue to grow in and waste products to flow out.

Conclusions

In this work, a resorbable phosphate glass (ICEL2) was synthesized and characterized to investigate its suitability for bone tissue repair. The glass solubility was investigated during a time span of 4 months by using distilled water, SBF and Tris-HCl as testing solutions. ICEL2 glass showed to be resorbable and underwent a process of congruent dissolution produced by a surface erosion mechanism. The dissolution rate was both medium- and time-dependent; maximum dissolution occurred in distilled water, wherein the glass lost almost 76 wt.% after 4 months of immersion, whereas the concomitant formation of a HA-like layer was observed on the surface of the samples treated in SBF and Tris-HCl, which demonstrated that the material was both bioactive and resorbable.

ICEL2 glass powder was used to prepare highly porous 3-D glass-ceramic scaffolds by means of the PE burning-out method. During the heat treatment, the polymeric phase burnt-out while the glass crystallized and sintered, thereby forming a glass-ceramic structure. Scaffolds

exhibiting a 3-D network of open and highly interconnected macropores, with a trabecular architecture analogous to that of cancellous bone, were obtained. A total pore content of about 87 vol.%, including both large (100-400 μm) and mid to small macropores (below 50 μm), was achieved. The compressive strength of the scaffolds was about 1.5 MPa, that is acceptable for bone tissue engineering applications. The scaffolds were highly soluble and lost about 76 wt.% after 4 months of soaking in SBF. During immersion, the struts between the pores became thinner and sometimes they completely disappeared due to a surface erosion mechanism, leading to pores enlargement and opening. The pH of SBF during the time frame of analysis varied between 7.30-7.55, i.e. between the optimal limits for bone cells viability, which further suggests the suitability of ICEL2 scaffolds for bone tissue engineering applications.

Acknowledgements

This work was partially funded by the EU IntraEuropean Marie Curie fellowship (BIORESS GA 210362) and Regione Piemonte (Ricerca Sanitaria Finalizzata 2008).

References

[1] Jones JR, Gentleman E and Polak J. Bioactive glass scaffolds for bone regeneration. *Elements* 2007; 3: 393-399.

[2] Gerhardt LC and Boccaccini AR. Bioactive glass and glass-ceramic scaffolds for bone tissue engineering. *Materials* 2010; 3: 3867-3910.

[3] Baino F and Vitale-Brovarone C. Three-dimensional glass-derived scaffolds for bone tissue engineering: current trends and forecasts for the future. *J Biomed Mater Res A* 2011; 97: 514-535.

[4] Rahaman MN, Day DE, Bal BS, Fu Q, Jung SB, Bonewald LF and Tomsia AP. Bioactive glass in tissue engineering, *Acta Biomater* 2011; 7: 2355-2373.

[5] Vitale-Brovarone C, Baino F, Tallia F, Gervasio C, Verné E. Bioactive glass-derived trabecular coating: a smart solution for enhancing osteointegration of prosthetic elements. *J Mater Sci: Mater Med* 2012; 23: 2369-2380.

[6] Jones JR. Review of bioactive glass: from Hench to hybrids. *Acta Biomater* 2013; 9: 4457-4486.

[7] Hench LL. The story of Bioglass®. *J Mater Sci: Mater Med* 2006; 17: 967-978.

[8] Salih V, Franks K, James M, Hastings GW and Knowles JC. Development of soluble glasses for biomedical use – Part II: the biological response of human osteoblast cell lines to phosphate-based soluble glasses. *J Mater Sci: Mater Med* 2000; 11: 615-620.

[9] Tadjoedin ES, De Lange GL, Holzmann PJ, Kuiper L and Burger EH. Histological observations on biopsies harvested following sinus floor elevation using a bioactive glass material of narrow size range. *Clin Oral Implants Res* 2000; 11: 334-344.

[10] Tadjoedin ES, De Lange GL, Lyaruu DM, Kuiper L and Burger EH. High concentrations of bioactive glass material (BioGran) vs. autogenous bone for sinus floor elevation. *Clin Oral Implants Res* 2002; 13: 428-436.

[11] Knowles JC. Phosphate based glasses for biomedical applications. *J Mater Chem* 2003; 13: 2395-2401.

[12] Bunker BC, Arnold GW and Wilder JA. Phosphate glass dissolution in aqueous solutions. *J Non-Cryst Solids* 1984; 64: 291-316.

[13] Abou Neel EA, Ahmed I, Blaker JJ, Bismarck A, Boccaccini AR, Lewis MP, Nazhat SN and Knowles JC. Effect of iron on the surface, degradation and ion release properties of phosphate-based glass fibres. *Acta Biomater* 2005; 1: 553-563.

[14] Abou Neel EA, Ahmed I, Pratten J, Nazhat SN and Knowles JC. Characterisation of antibacterial copper releasing degradable phosphate glass fibres. *Biomaterials* 2005; 26: 2247-2254.

[15] Abou Neel EA and Knowles JC. Physical and biocompatibility studies of novel titanium dioxide doped phosphate-based glasses for bone tissue engineering applications. *J Mater Sci: Mater Med* 2008; 19: 377-386.

[16] Abou Neel EA, Pickup DM, Valappil SP, Newport RJ and Knowles JC. Bioactive functional materials: a perspective on phosphate-based glasses. *J Mater Chem* 2009; 19: 690-701.

[17] Jeans LA, Gilchrist T and Healy D. Peripheral nerve repair by means of flexible biodegradable glass fibre wrap: a comparison with microsurgical epineuril repair. *J Plast Reconstr Aesthet Surg* 2007; 60: 1302-1308.

[18] Vitale-Brovarone C, Novajra G, Lousteau J, Milanese D, Raimondo S and Fornaro M. Phosphate glass fibres and their role in neuronal polarization and axonal growth direction. *Acta Biomater* 2012; 8: 1125-1136.

[19] Shah R, Sinanan ACM, Knowles JC, Hunt NP and Lewis MP. Craniofacial muscle engineering using a 3-dimensional phosphate glass fibre construct. *Biomaterials* 2005; 26: 1497-1505.

[20] Lakhkar NJ, Lee IH, Kim HW, Salih V, Wall IB and Knowles JC. Bone formation controlled by biologically relevant inorganic ions: role and controlled delivery from phosphate-based glasses. *Adv Drug Delivery Rev* 2013; 65:405-420.

[21] Hutmacher DW. Scaffolds in tissue engineering bone and cartilage. *Biomaterials* 2000; 21: 2529-2543.

[22] Jones J and Hench LL. Regeneration of trabecular bone using porous ceramics. *Curr Opin Solid State Mater Sci* 2003; 7: 301-307.

[23] Gauthier O, Bouler JM, Aguado E, Pilet P and Daculsi G. Macroporous biphasic calcium phosphate ceramics: influence of macropore diameter and macroporosity percentage on bone ingrowth. *Biomaterials* 1998; 19: 133-139.

[24] Karageorgiou V and Kaplan D. Porosity of 3D biomaterial scaffolds and osteogenesis. *Biomaterials* 2005; 26: 5474-5491.

[25] Lyckfeldt O and Ferreira MF. Processing of porous ceramics by starch consolidation. *J Eur Ceram Soc* 1998; 18: 131-140.

[26] Vitale-Brovarone C, Di Nunzio S, Bretcanu O and Verné E. Macroporous glass-ceramic materials with bioactive properties. *J Mater Sci: Mater Med* 2004; 15: 209-217.

[27] Yuan H, De Buijin JD, Zhang X, Van Blitterswijk CA and De Groot K. Bone induction by porous glass ceramic made from Bioglass® (45S5). *J Biomed Mater Res (Appl Biomater)* 2001; 58: 270-276.

[28] Sepulveda P, Binner JGP, Rogero SO, Higa OZ and Bressiani JC. Production of porous hydroxyaptite by the gel-casting of foams and cytotoxic evaluation. *J Biomed Mater Res* 2000; 50: 27-34.

[29] Gough JE, Jones JR and Hench LL. Nodule formation and mineralization of human primary osteoblasts cultured on a porous bioactive glass scaffold. *Biomaterials* 2004; 25: 2039-2046.

[30] Chen QZ, Thompson ID and Boccaccini AR. 45S5 Bioglass®-derived glass-ceramic scaffolds for bone tissue engineering. *Biomaterials* 2006; 27: 2414-2425.

[31] Vitale-Brovarone C, Verné E, Robiglio L, Appendino P, Bassi F, Martinasso G, Muzio G and Canuto R. Development of glass-ceramic scaffolds for bone tissue engineering: characterisation, proliferation of human osteoblasts and nodule formation. *Acta Biomater* 2007; 3: 199-208.

[32] Vitale-Brovarone C, Miola M, Balagna C and Verné E. 3D-glass-ceramic scaffolds with antibacterial properties for bone grafting. *Chem Eng J* 2008; 137: 129-136.

[33] Vitale-Brovarone C, Baino F and Verné E. High strength bioactive glass-ceramic scaffolds for bone regeneration. *J Mater Sci: Mater Med* 2009; 20: 643-653.

[34] Baino F, Ferraris M, Bretcanu O, Verné E and Vitale-Brovarone C. Optimization of composition, structure and mechanical strength of bioactive 3-D glass-ceramic scaffolds for bone substitution. *J Biomater Appl* 2013; 27: 872-890.

[35] Renghini C, Giuliani A, Mazzoni S, Brun F, Larsson E, Baino F and Vitale-Brovarone C. Microstructural characterization and in vitro bioactivity of porous glass-ceramic scaffolds for bone regeneration by synchrotron radiation X-ray microtomography. *J Eur Ceram Soc* 2013; 33: 1553-1565.

[36] Ramay HR and Zhang M. Preparation of porous hydroxyapatite scaffolds by combination of the gel-casting and polymer sponge method. *Biomaterials* 2003; 24: 3293-3302.

[37] Vitale-Brovarone C, Verné E, Robiglio L, Martinasso G, Canuto RA and Muzio G. Biocompatible glass-ceramic materials for bone substitution. *J Mater Sci: Mater Med* 2008; 19: 471-478.

[38] Vitale-Brovarone C, Baino F, Miola M, Mortera R, Onida B and Verné E. Glass-ceramic scaffolds containing silica mesophases for bone grafting and drug delivery. *J Mater Sci: Mater Med* 2009; 20: 809-820.

[39] Baino F, Verné E and Vitale-Brovarone C. 3-D high strength glass-ceramic scaffolds containing fluoroapatite for load-bearing bone portions replacement. *Mater Sci Eng C* 2009; 29: 2055-2062.

[40] Bellucci D, Cannillo V, Sola A, Chiellini F, Gazzarri M and Migone C. Macroporous Bioglass®-derived scaffolds for bone tissue regeneration. *Ceram Int* 2011; 37: 1575-1585.

[41] Navarro M, Del Valle S and Martinez S. New macroporous calcium phosphate glass-ceramic for guided bone regeneration. *Biomaterials* 2004; 25: 4233-4241.

[42] Park YS, Kim KN and Kim KM. Feasibility of three dimensional macroporous scaffold using calcium phosphate glass and polyurethane sponge. *J Mater Sci: Mater Med* 2006; 41: 4357-4364.

[43] Vitale-Brovarone C, Baino F, Bretcanu O and Vernè E. Foam-like scaffolds for bone tissue engineering based on a novel couple of silicate-phosphate specular glasses: synthesis and properties. *J Mater Sci: Mater Med* 2009; 20: 2197-2205.

[44] Vitale-Brovarone C, Ciapetti G, Leonardi E, Baldini N, Bretcanu O, Verné E and Baino F. Resorbable glass-ceramic phosphate-based scaffolds for bone tissue engineering: synthesis, properties and in vitro effects on human marrow stromal cells. *J Biomater Appl* 2011; 26: 465-489.

[45] Gentile P, Chiono V, Tonda-Turo C, Mattu C, Baino F, Vitale-Brovarone C and Ciardelli G Bioresorbable glass effect on the physico-chemical properties of bilayered scaffolds for osteochondral regeneration. *Mater Lett* 2012; 89: 74-76.

[46] ISO 10993-14:2002. Biological evaluation of medical devices: identification and quantification of degradation products from ceramics.

[47] Kokubo T and Takadama H. How useful is SBF in predicting in vivo bone bioactivity?. *Biomaterials* 2006; 27:2907-2915.

[48] Kenesei P, Kadar C, Rajkovits Z and Lendvai J. The influence of cell-size distribution on the plastic deformation in metal foams. *Scripta Mater* 2004; 50: 295-300.

[49] Renghini C, Komlev V, Fiori F, Verné E, Baino F and Vitale-Brovarone C. Micro-CT studies on 3-D bioactive glass-ceramic scaffolds for bone regeneration. *Acta Biomater* 2009; 5: 1328-1337.

[50] Muzio G, Verné E, Canuto RA, Martinasso G, Saracino S, Baino F, Miola M, Berta L, Frairia R and Vitale-Brovarone C. Shock waves induce activity of human osteoblast-like cells in bioactive scaffolds. *J Trauma Injury Infection Crit Care* 2010; 68: 1439-1444.

[51] Hoppe A, Güldal NG and Boccaccini AR. A review of the biological response to ionic dissolution products from bioactive glasses and glass-ceramics. *Biomaterials* 2011; 32: 2757-2774.

[52] Patel A and Knowles JC. Investigation of silica-iron-phosphates glasses for tissue engineering. *J Mater Sci: Mater Med* 2006; 17: 937-944.

[53] Hench LL. Genetic design of bioactive glasses. *J Eur Ceram Soc* 2009; 29: 1257-1265.

[54] Hruby A. Evaluation of glass-forming tendency by means of DTA. *Czech J Phys* 1972; 22 : 1187-1193.

[55] Lara C, Pascual MJ and Duran A. Glass-forming ability, sinterability and thermal properties in the system RO-BaO-SiO_2 (R = Mg, Zn). *J Non-Cryst Solids* 2004; 348: 149-155.

[56] Bretcanu O, Chatzistavrou X, Paraskevpoulos K, Conradt R, Thompson I and Boccaccini AR. Sintering and crystallization of 45S5 Bioglass® powder. *J Eur Ceram Soc* 2009; 29: 3299-3306.

[57] Kansal I, Tulyaganov DU, Goel A, Pascual MJ and Ferreira JMF. Structural analysis and thermal behavior of diopside-fluorapatite-wollastonite-based glasses and glass–ceramics. *Acta Biomater* 2010; 6: 4380-4388.

[58] Clement J, Manero JM, Planell JA, Avial G and Martinez S. Analysis of the structural change of a phosphate glass during its dissolution in simulated body fluid. *J Mater Sci: Mater Med* 1999; 10: 729-732.

[59] Gao H, Tan T and Wang D. Dissolution mechanism and release kinetics of phosphate controlled release glasses in aqueous medium. *J Controll Rel* 2004; 96: 29-36.

[60] Franks K, Abrahams I and Knowles JC. Development of soluble glasses for biomedical use. Part I: In vitro solubility measurement. *J Mater Sci: Mater Med* 2000; 11: 609-614.

[61] Delahaye F, Montagne L, Palavit G, Touray JC and Baillif P. Acid dissolution of sodium calcium metaphosphate glasses. *J Non-Cryst Solids* 1998; 242: 25-32.

[62] Leonardi E, Ciapetti G, Baldini N, Novajra G, Verné E, Baino F and Vitale-Brovarone C. Response of human bone marrow stromal cells to a resorbable P_2O_5-SiO_2-CaO-MgO-Na_2O-K_2O phosphate glass-ceramic for tissue engineering applications. *Acta Biomater* 2010; 6: 598-606.

[63] Chor MV and Li W. A permeability measurement system for tissue engineering scaffolds. *Meas Sci Technol* 2007; 18: 208-216.

[64] She FH, Tung KL and Kong LX. Calculation of effective pore diameters in porous filtration membranes with image analysis. *Robotics Computer-Integrated Manufact* 2008; 24: 427-434.

[65] Kohles SS, Roberts JB, Upton ML, Wilson CG, Bonassar LJ and Schlichting AL. Direct perfusion measurements of cancellous bone anisotropic permeability. *J Biomech* 2004; 34: 1197-1202.

[66] Nauman EA, Fong KE and Keaveny TM. Dependence of intertrabecular permeability on flow direction and anatomic site. *Ann Biomed Eng* 1999; 27: 517-524.

[67] Shimko DA, Shimkon VF, Sander EA, Dickson KF and Nauman EA. Effect of porosity on the fluid flow characteristics and mechanical properties of tantalum scaffolds. *J Biomed Mater Res B* 2005; 73: 315-324.

[68] Li S, De Wijn JR, Li J, Layrolle P and De Groot K. Macroporous biphasic calcium phosphate scaffolds with high permeability/porosity ratio. *Tissue Eng* 2003; 9: 535-546.

[69] Ochoa I, Sanz-Herrera J, Garica-Aznar J, Doblaré M, Yunos D and Boccaccini AR. Permeability evaluation of 45S5 Bioglass®-based scaffolds for bone tissue engineering. *J Biomech* 2009; 42: 257-260.

[70] Jones JR, Poologasundarampillai G, Atwood RC, Bernard D and Lee P. Non-destructive quantitative 3D analysis for the optimisation of tissue scaffolds. *Biomaterials* 2007; 28: 1404-1413.

[71] Jones JR, Atwood RC, Poologasundarampillai G, Yue S and Lee PD. Quantifying the 3D macrostructure of tissue scaffolds. *J Mater Sci: Mater Med* 2009; 20: 463-471.

[72] Hench LL. Bioceramics: from concept to clinic. *J Am Ceram Soc* 1991; 74: 1487-1510.

[73] Bretcanu O, Chen Q, Misra SK, Boccaccini AR, Verné E and Vitale-Brovarone C. Biodegradable polymer coated 45S5 Bioglass-derived glass-ceramic scaffolds for bone tissue engineering. *Glass Tech Eur J Glass Sci Tech A* 2007; 48: 227-234.

[74] Chen QZ and Boccaccini AR. Poly(D, L-lactic acid) coated 45S5 Bioglass®-based scaffolds: processing and characterization. *J Biomed Mater Res A* 2006; 77: 445-457.

[75] Baino F, Verne E and Vitale-Brovarone C. Feasibility, tailoring and properties of polyurethane/bioactive glass composite scaffolds for tissue engineering. *J Mater Sci: Mater Med* 2009; 20: 2189-2195.

[76] Martinez-Vazquez FJ, Perera FH, Miranda P, Pajares A and Guiberteau F. Improving the compressive strength of bioceramic robocast scaffolds by polymer infiltration. *Acta Biomater* 2010; 6: 4361-4368.

[77] Woodard JR, Hilldore AJ, Lan SK, Park CJ, Morgan AW, Eurell JA, Clark SG, Wheeler MB, Jamison RD and Wagoner Johnson AJ. The mechanical properties and osteoconductivity of hydroxyapatite bone scaffolds with multi-scale porosity. *Biomaterials* 2007; 28: 45-54.

[78] Liu X, Rahaman MN and Fu Q. Bone regeneration in strong porous bioactive glass (13-93) scaffolds with an oriented microstructure implanted in rat calvarial defects. *Acta Biomater* 2013; 9: 4889-4898.

[79] Kaysinger KK and Ramp WR. Extracellular pH modulates the activity of cultured human osteoblasts. *J Cell Biochem* 1998; 68: 83-89.

Figure legends

Figure 1. XRD patterns of (a) ICEL2 glass and (b) ICEL2-derived scaffold after thermal treatment at 550 °C/3 h.

Figure 2. Differential scanning calorimetry (DSC) plot of ICEL2 glass.

Figure 3. Shrinkage of ICEL2 glass obtained by hot stage microscopy (HSM).

Figure 4. Digital camera images of ICEL2 glass samples before (right side) and after (left side) soaking in different testing media for 4 months: (a) distilled water, (b) Tris-HCl, (c) SBF.

Figure 5. Weight losses of ICEL2 glass samples during immersion in three testing media (distilled water, Tris-HCl and SBF) for different time frames.

Figure 6. Weight loss per unit surface of ICEL2 glass samples during immersion in distilled water: experimental data (continuous line) and fitting linear curve (dashed line).

Figure 7. ICEL2 scaffolds: (a) green body (compact body of pressed glass and PE particles; sample diameter 30 mm); (b) ICEL2-derived scaffold as extracted from the furnace (after thermal treatment at 550 °C/3 h); (c) ICEL2 scaffold after cutting into a regular cubic shape; (d) SEM micrograph of the scaffold (magnification 300×).

Figure 8. Capillarity test: (a-f) phases of the test carried out on a ICEL2 scaffold; (g) comparison of the samples before (left side) and after (right side) the test; (h) cross-sections of the scaffolds before (left side) and after (right side) the test.

Figure 9. Compressive stress-strain curve of ICEL2 scaffolds.

Figure 10. Weight losses of ICEL2 scaffolds during immersion in SBF for different time frames.

Figure 11. Low-magnification SEM micrographs of ICEL2 scaffolds (a) before and (b) after soaking for 2 months in SBF (magnification 50× in both cases); (c) high-magnification (1000×) SEM image of scaffold struts showing the presence of a newly formed phases with the relevant compositional analysis by EDS (d).

Figure 12. Image analysis: (a) pore size distribution and (b) pores area of ICEL2 scaffold before and after soaking for 2 months in SBF.

Tables

Table 1. Comparison of thermal parameters among ICEL2 and other biomedical glasses (data available in the literature).

Material	Powder size (μm)	δ (°C)	K_H	S_c (°C)	References
ICEL2	< 32	140	1.4	80	Present work
CEL2	< 32	100	0.28	0	[34]
45S5 Bioglass®	< 32	37	0.066	< 0	[34]
	< 5 (commercial powders)	64	0.25	< 0	[56]
Glasses in the CaO-MgO-SiO_2-P_2O_5-Na_2O-CaF_2 system	~10	-	-	74-99	[57]

Table 2. Comparison of porosity and mechanical properties of selected bone tissue engineering scaffolds fabricated by PE burning-out and sponge replication techniques.

System and composition (mol.%) of the starting glass	Glass family[a]	Fabrication method	Porosity (vol.%)	Compressive strength (MPa)	References
$45P_2O_5$-26CaO-$15Na_2O$-$3SiO_2$-$4K_2O$-7MgO (ICEL2)	P	Sponge replication	85	0.4	[43,44]
		PE burning-out	87	1.5	Present work
$45SiO_2$-26CaO-$15Na_2O$-$3P_2O_5$-$4K_2O$-7MgO (CEL2)	S	Sponge replication	55-75 [b]	1.0-5.5 [b]	[33,34,43]
		PE burning-out	48	7	[37]
$50SiO_2$-18CaO-$7Na_2O$-$6P_2O_5$-$7K_2O$-3MgO-$9CaF_2$ (FaGC)	S	Sponge replication	75	2	[32]
		PE burning-out	23.5-50.0 [b]	20.0-150.0 [b,c]	[38,39]
$46.1SiO_2$-26.9CaO-$24.4Na_2O$-$2.6P_2O_5$ (45S5 Bioglass®)	S	Sponge replication	70-90 [b]	0.4-2.5 [b]	[30,34]
		PE burning-out	60-70 [b]	117.7-123.2 [b]	[40]

[a] P = phosphate glass; S = silicate glass.
[b] Different scaffolds batches were produced by varying the processing parameters in a controlled way (see the related references for details).
[c] The scaffolds were mechanically anisotropic (different strength were registered if the load was applied along the compaction direction or along a transversal direction).

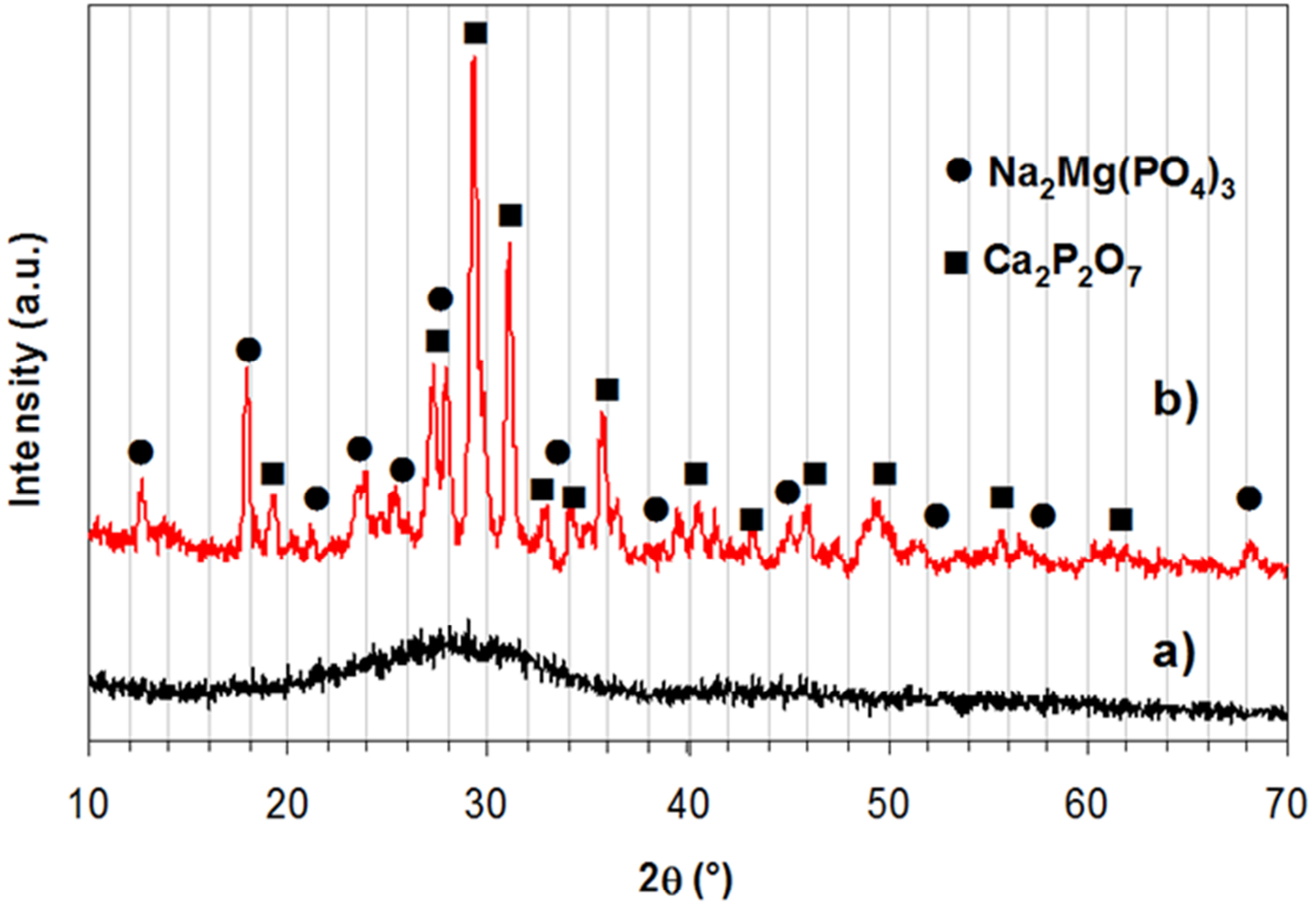

Fig. 1

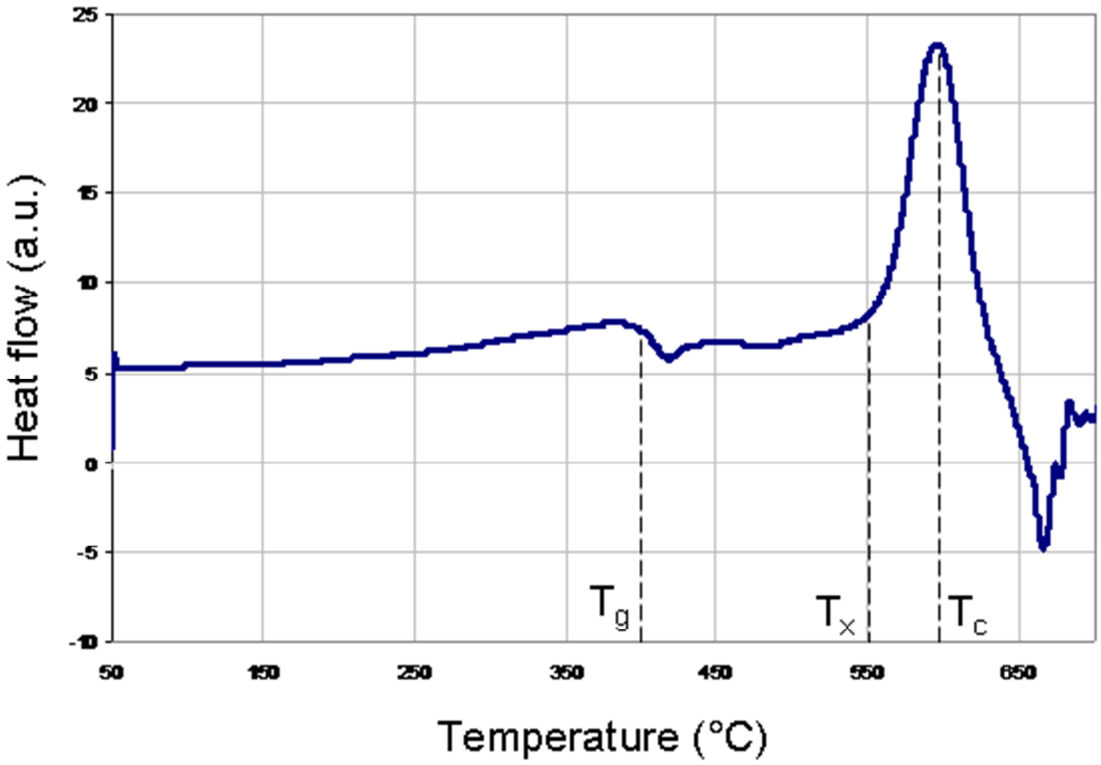
Heat flow (a.u.)
25
20
15
10
5
0
-5
-10
50
150
250
350
450
550
650
Temperature (°C)
T_g
T_x
T_c

Fig. 2

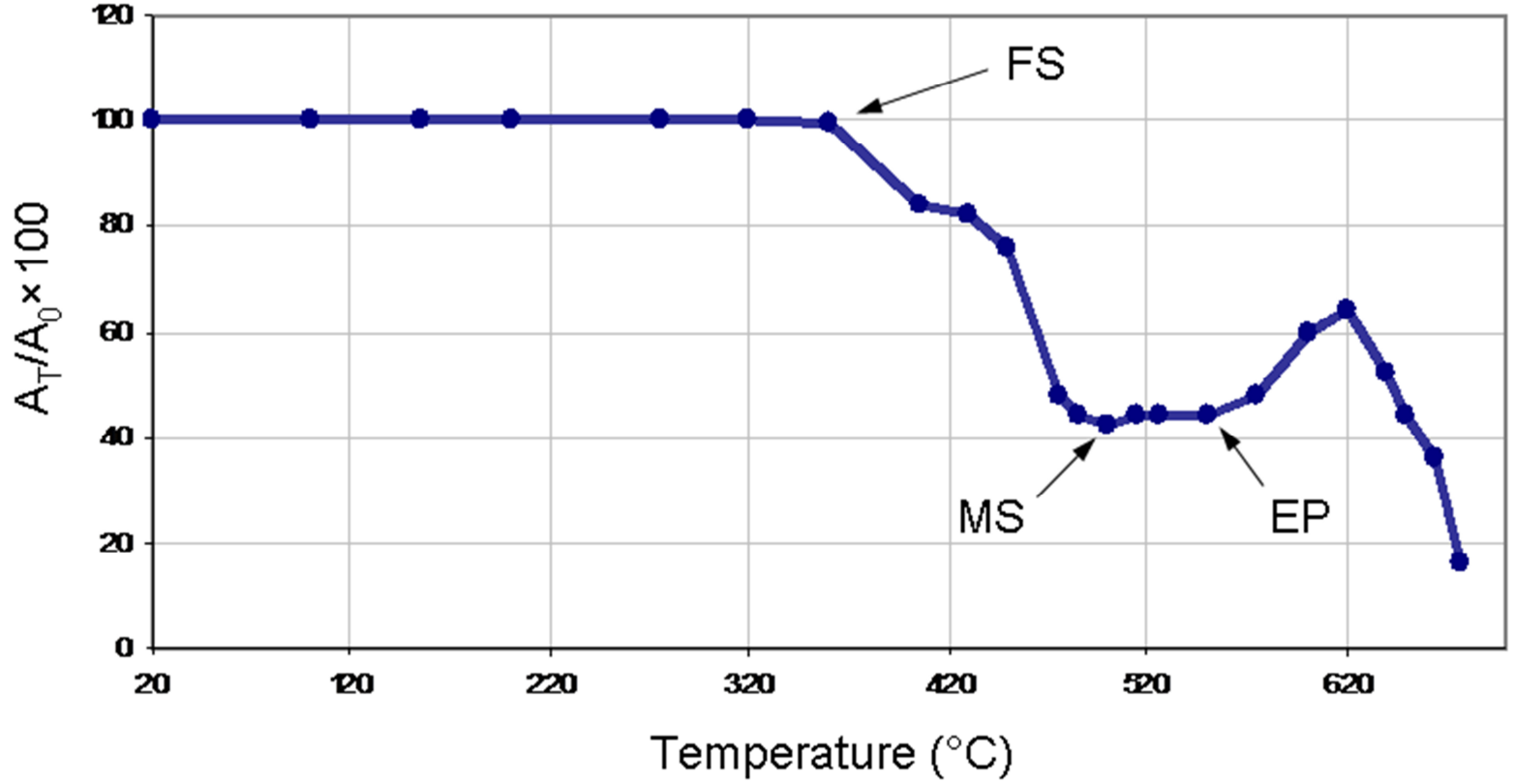
120
100
80
60
40
20
0
$A_T/A_0 \times 100$
FS
MS
EP
20
120
220
320
420
520
620
Temperature (°C)

Fig. 3

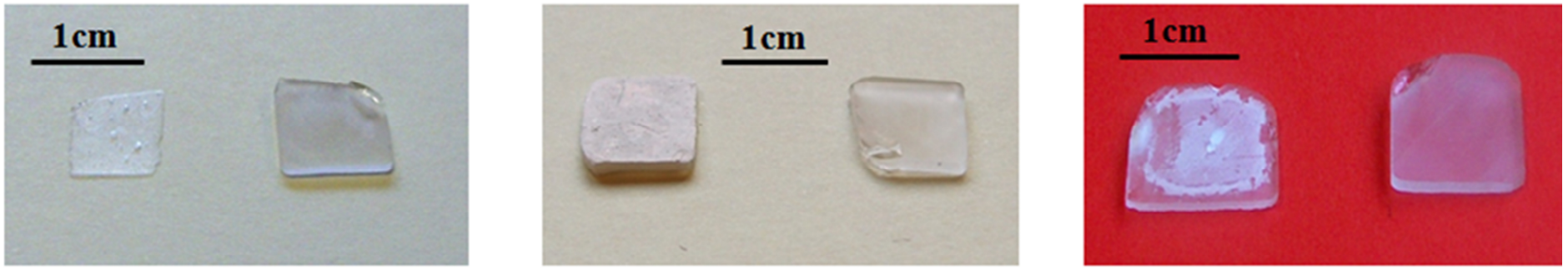

Fig. 4

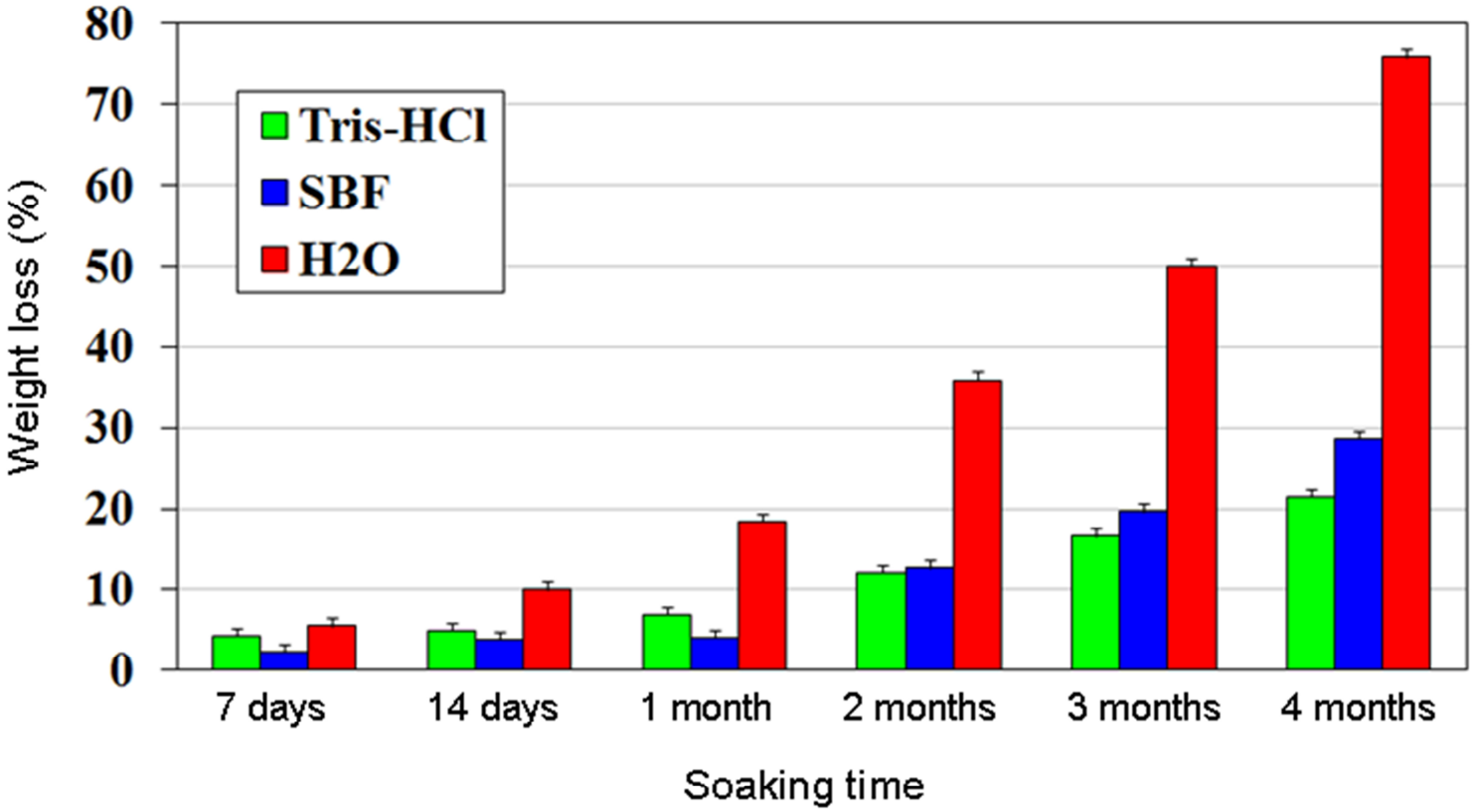
80
70
60
50
40
30
20
10
0
Weight loss (%)
Tris-HCl
SBF
H2O
7 days
14 days
1 month
2 months
3 months
4 months
Soaking time

Fig. 5

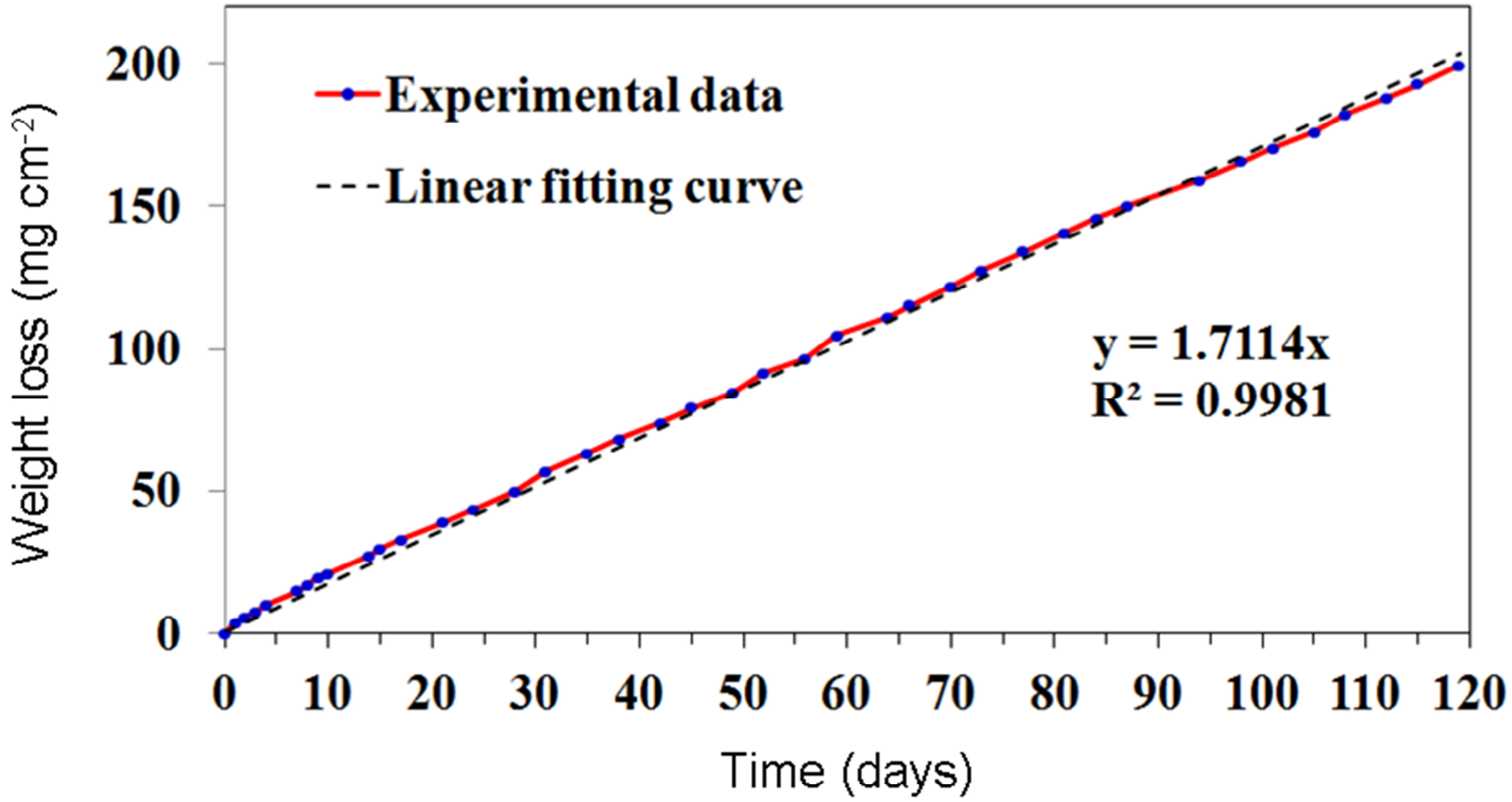
Experimental data
Linear fitting curve
y = 1.7114x
R² = 0.9981
Weight loss (mg cm-2)
Time (days)
0
50
100
150
200
0
10
20
30
40
50
60
70
80
90
100
110
120

Fig. 6

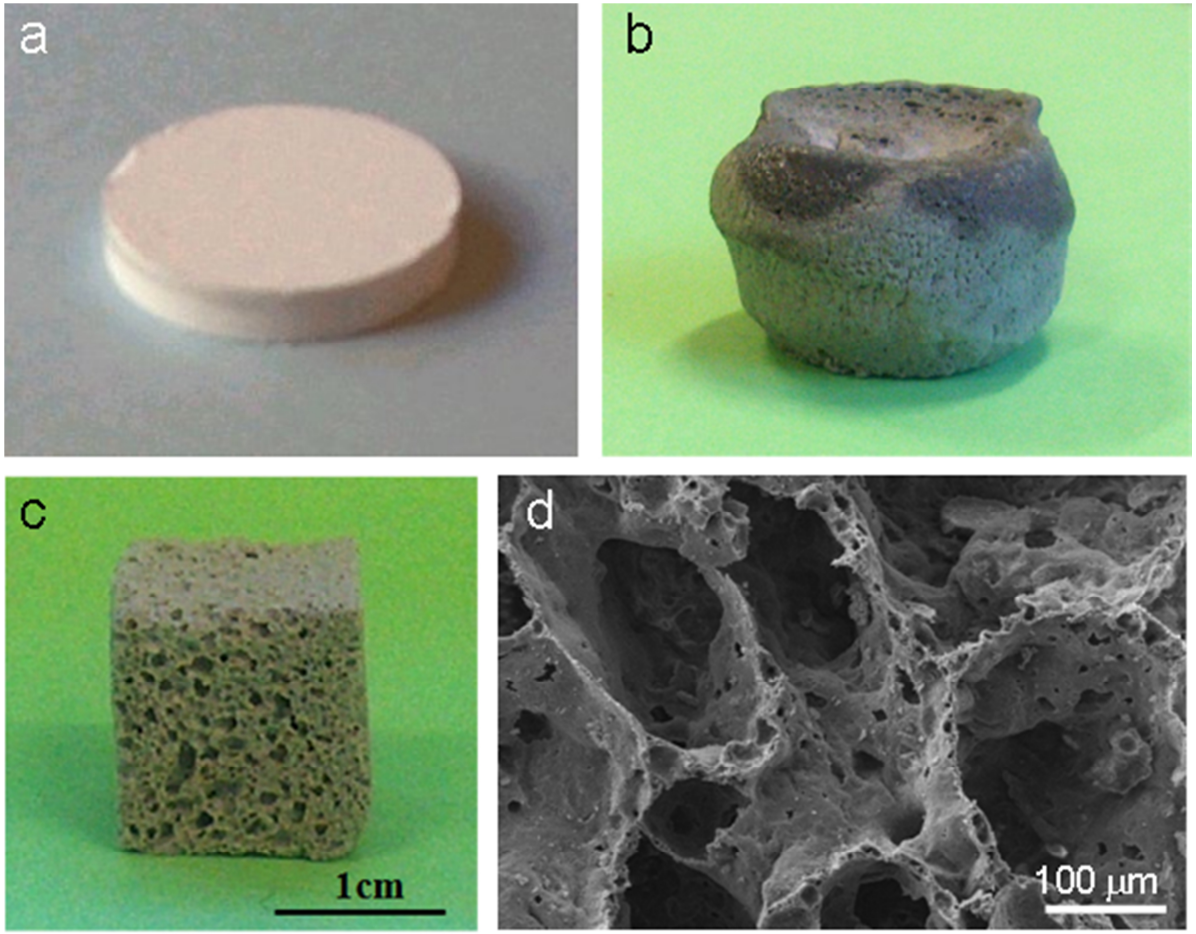

Fig. 7

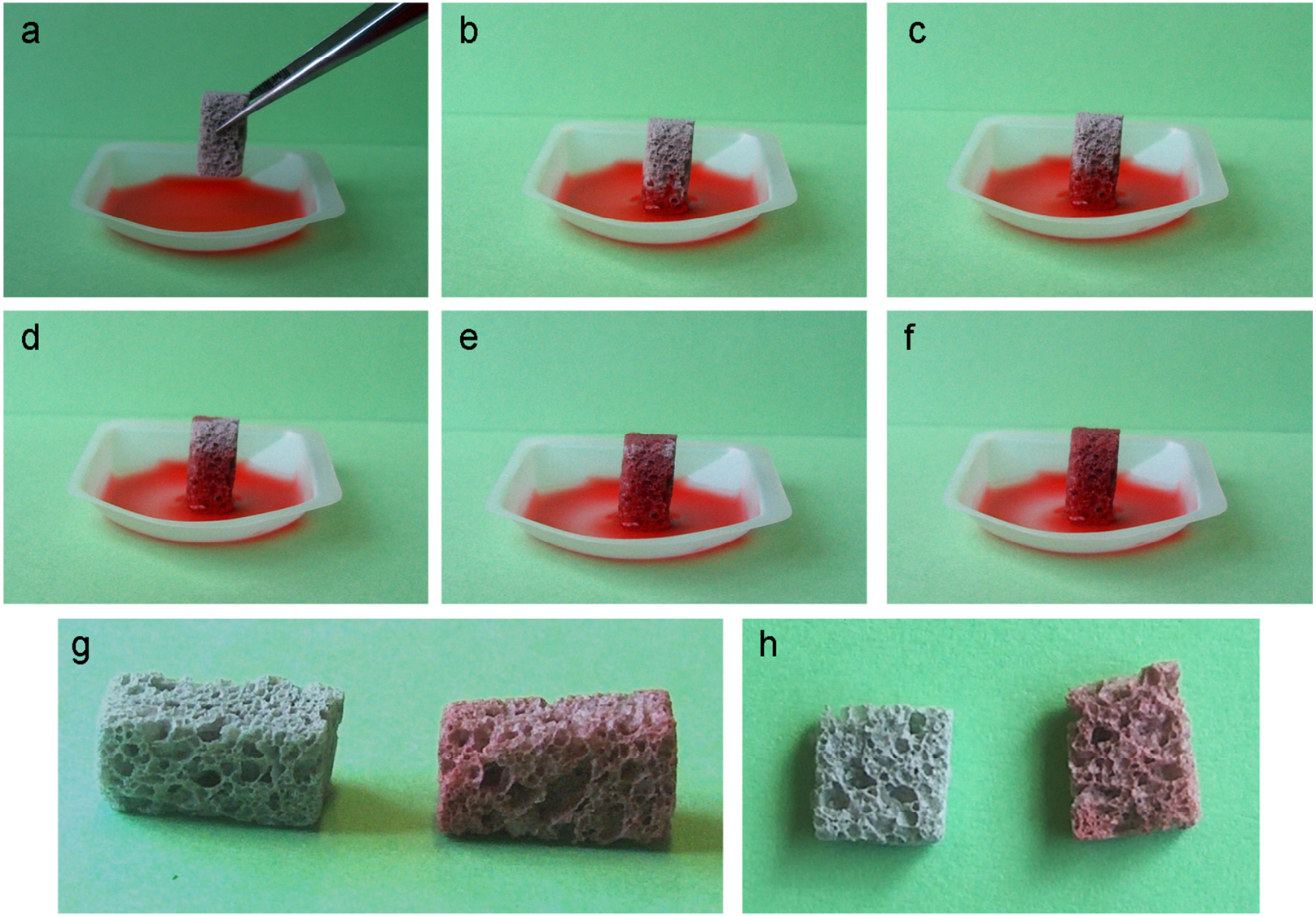

Fig. 8

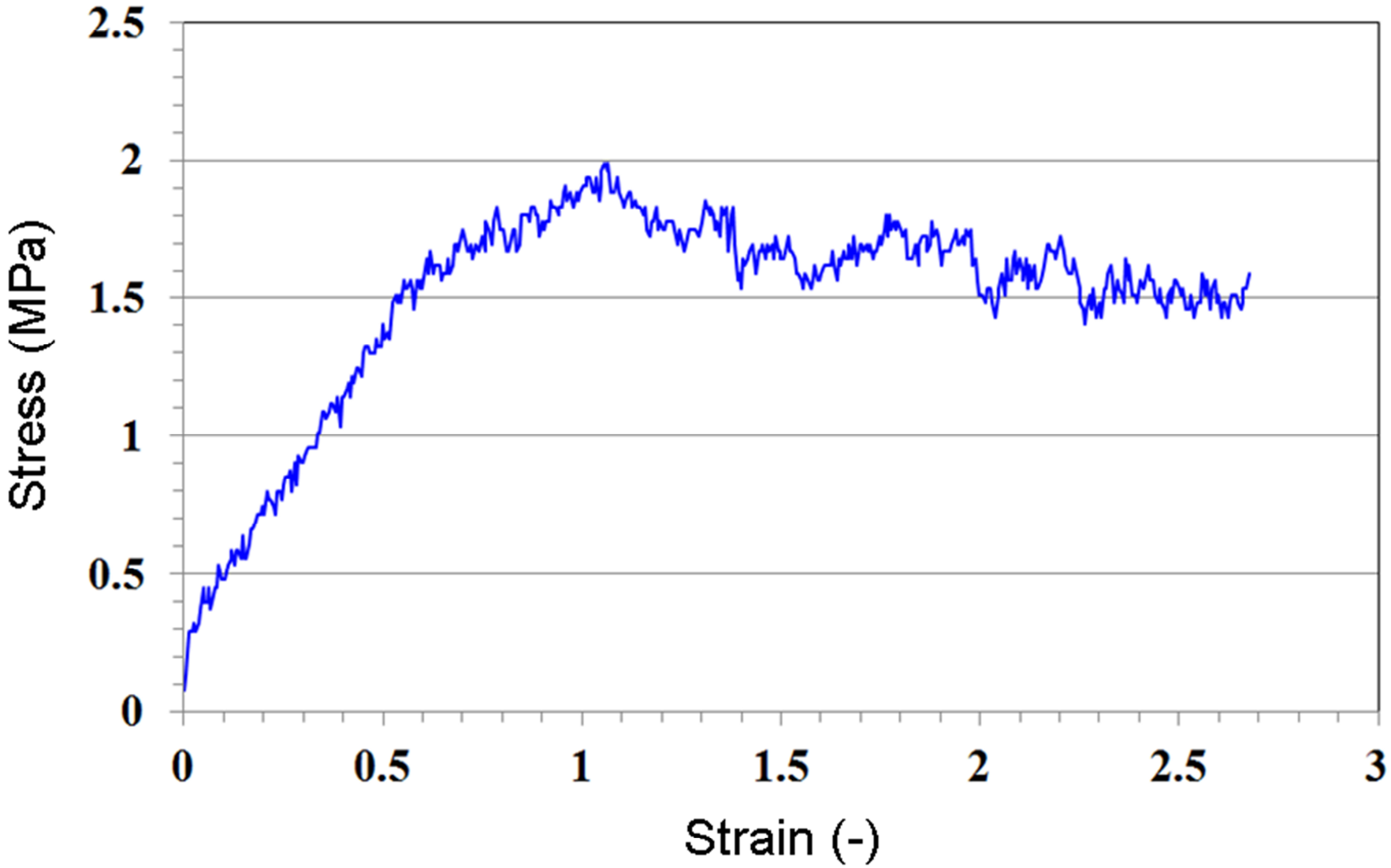

Fig. 9

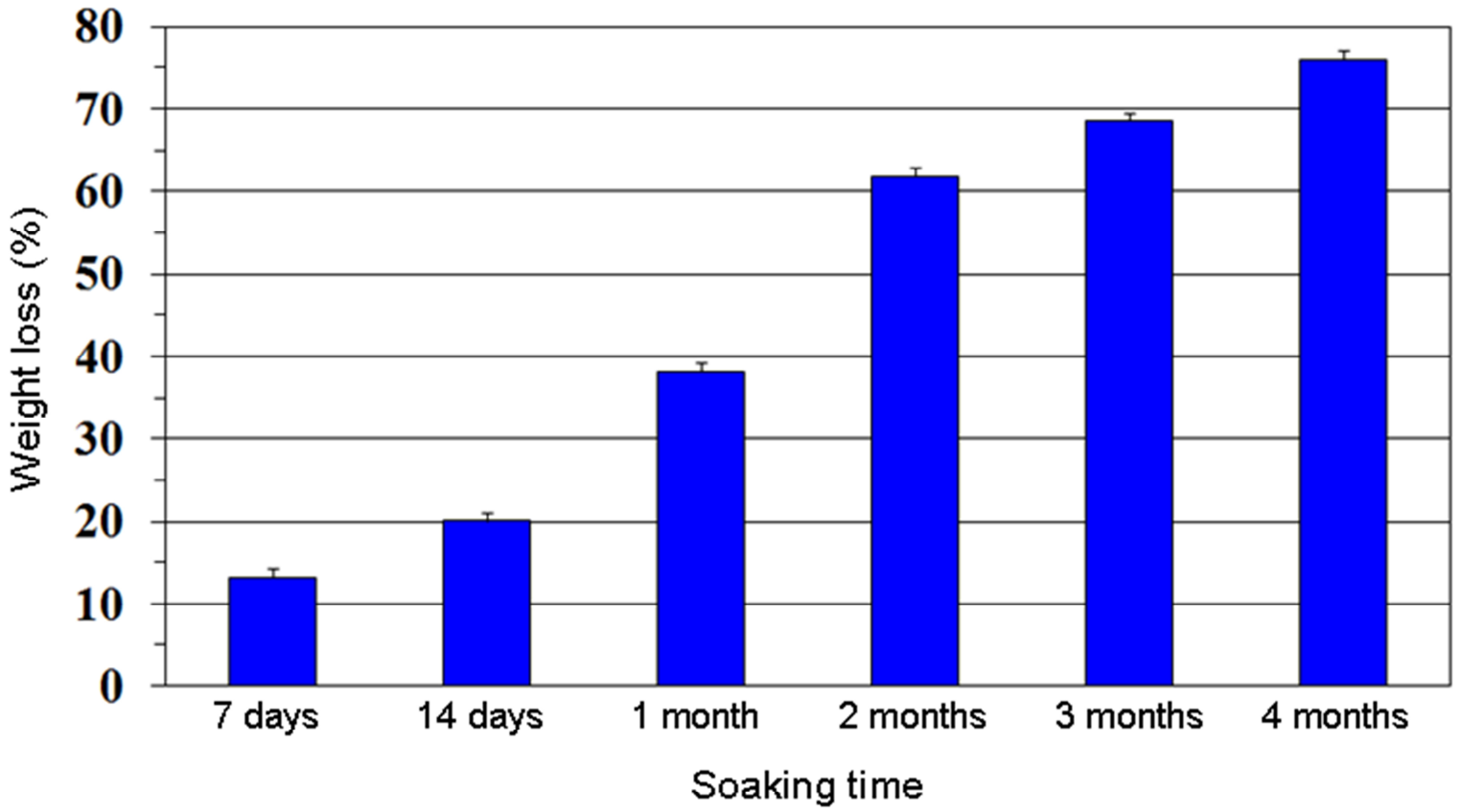
80
70
60
50
40
30
20
10
0
Weight loss (%)
7 days
14 days
1 month
2 months
3 months
4 months
Soaking time

Fig. 10

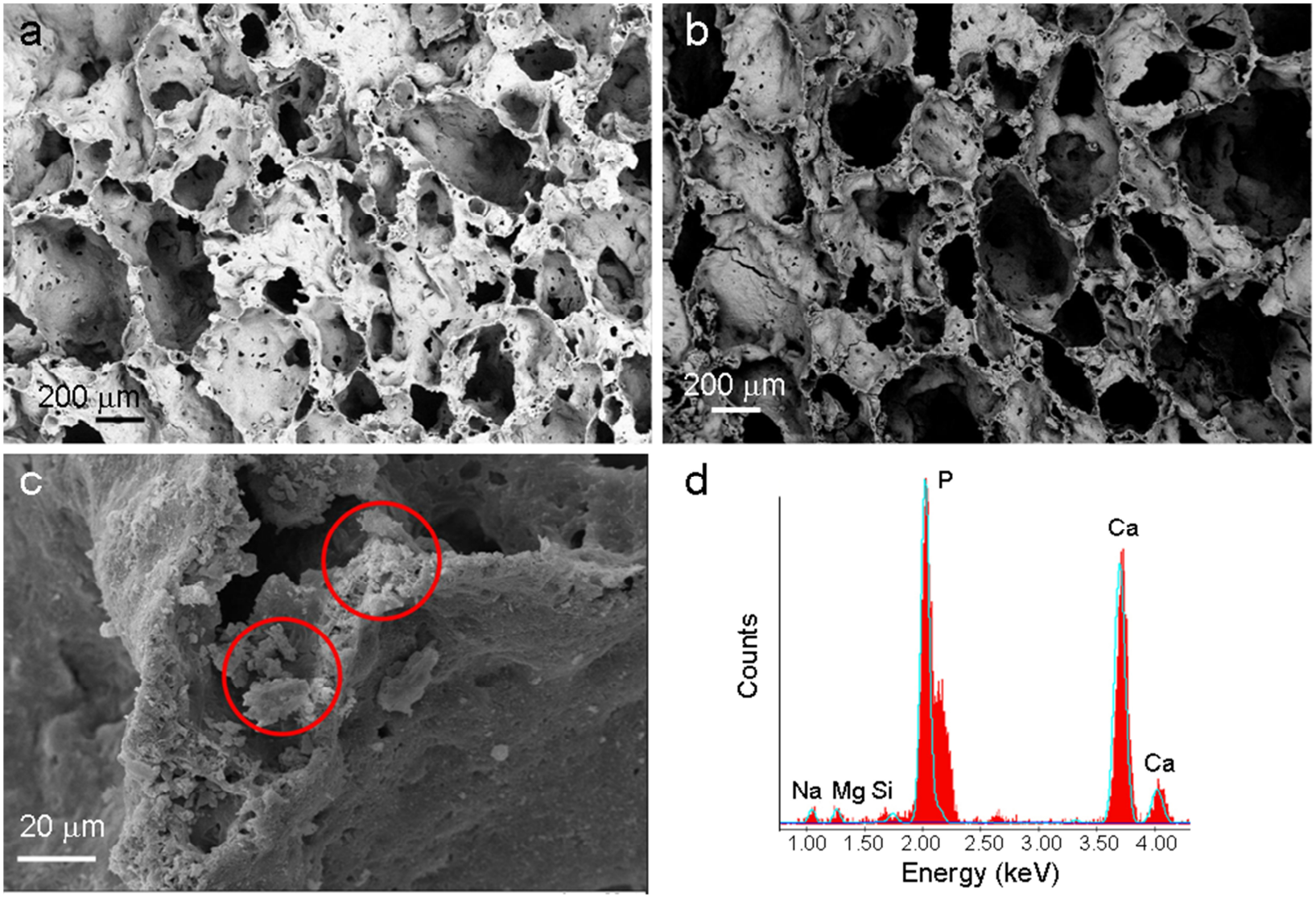
a
200 µm
b
200 µm
c
20 µm
d
P
Ca
Ca
Na Mg Si
Counts
1.00 1.50 2.00 2.50 3.00 3.50 4.00
Energy (keV)

Fig. 11

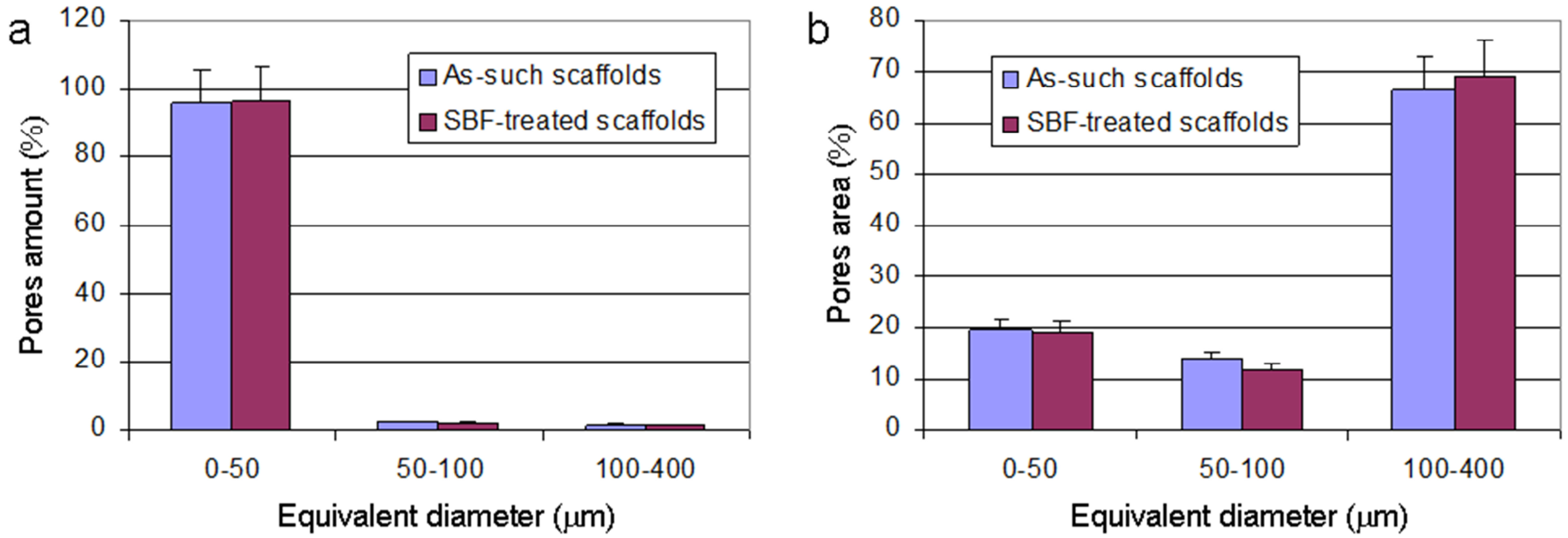
a
Pores amount (%)
120
100
80
60
40
20
0
As-such scaffolds
SBF-treated scaffolds
0-50
50-100
100-400
Equivalent diameter (μm)
b
Pores area (%)
80
70
60
50
40
30
20
10
0
As-such scaffolds
SBF-treated scaffolds
0-50
50-100
100-400
Equivalent diameter (μm)

Fig. 12